Nagel-Schreckenberg-Based Signalised Intersection Models

by

A Thesis submitted to the School of Graduate Studies in partial fulfillment of the requirements for the degree of

Master of Applied Science

University of Toronto Institute for Aerospace Engineering

University of Toronto

January 2012

Toronto Ontario

Abstract

A signalised traffic intersection model is developed based on Nagel & Schreckenberg's [1992] single road model. The model is comprised of four lanes with additional rules causing cars to stop. In contrast to most existing signalised intersection models, cars occupy the cells shared between two lanes in this model. Expressions for traffic flow rates as a function of turn proportion are derived using a mean-field approximation (MFA). Deviations from the MFA at the intersection cells are necessary to ensure conservation of cars is obeyed in the approximation. Results are compared with simulation and measurements from a video-based traffic flow/turn count estimator. A time-averaged background frame is subtracted from individual frames to yield a movement frame. Fixed-size blob (car) detection on this movement frame provides the basis for blob tracking. The individual car detections in each frame are combined with detections from past and future frames using Reid's [1979] Multiple Hypothesis Tracking. Turns are detected by manual selection of each lane's polygon in a video frame; the lane (location) of origin and exit are mapped to left, right and nonturn decisions. Three approaches to calculating a flow-vs-turn-proportion relationship are attempted. Measurement, experiment and simulation all reflect a negative relationship between left turns and flow rate. Model simulation agrees with MFA results except at low proportions of left-turning cars and high proportions of right-turning cars, during which the MFA yields a lower estimate than the simulated flow.

Acknowledgements

Thank you to my supervisor, Dr. Gabriele D'Eleuterio and the Space Robotics group for valuable feedback on this project. Thank you to the following authors for making this code available. All existing scripts used in this project were made available to the public through various licenses.

- normxcorr2_mex: MATLAB wrapper for OpenCV normxcorr2. Written by Daniel Eaton
- cquiver.m: Vector field plotter. Written by Nicholas Howe, Andrew Roberts.
- k_best_assign.m and partition_node.m: Murty's Algorithm implementation by Eric Trautmann
- munkres.m: Munkres linear assignment implementation used in Murty's algorithm by Yi Cao
- elipse.m: Ellipse plotting for rendering position covariance ellipses by David Long

Table of Contents

List of Tables

List of Figures

Chapter 1

Background and Motivation

Traffic models mostly aim to relate the flow of vehicles to other factors—vehicle density or light timing, for example. The earliest models described the flow of traffic along single-lane highways. Newer models add multiple lanes, roundabouts, T-intersections and signalised intersections. These models usually postulate some behaviour of traffic at a local or individual vehicle scale and seek the corresponding relationship between macroscopic variables.

Intersection models can be used to predict the results of traffic rules (for example allowing left or right turns), generate more efficient light timing, and studying the sources of intersection phenomena like gridlock. In most signalised intersection models presented so far, certain interactions inside intersections are discarded or simplified. In some models, vehicles jump from an approach to an exit without occupying the shared road inside the intersection. In other cases, conflicting traffic streams do not occur during the same signal phase, thereby reducing the number of interactions occuring inside the intersection. For these reasons, existing intersection models do not reflect the effect of turn proportion on flow rate.

This thesis presents a signalised-intersection model which incorporates interactions inside intersections in more detail than existing models. These additional interactions define the

stopping rules for vehicles entering and inside the intersection. This allows examination of the effect of turn proportion on the vehicle flow rate at the intersection. The model consists of four intersecting lanes with rules prevent collisions and gridlock while allowing traffic to flow.

Existing traffic and intersection models are reviewed with attention to the treatment of cells inside the intersection and the turning behaviour of vehicles in this chapter. The intersection model presented in Chapter 2 is composed of four intersecting single-lane roads based on an existing model [Nagel & Schreckenberg 1992] plus additional rules governing the vehicles at or immediately before the cells in the intersection. These rules serve to prevent collisions while allowing vehicles to proceed through according to the normal rules of the road. Vehicles may turn left across oncoming traffic and turn right on red lights provided it will not result in a collision. One of the new rules is necessary to prevent gridlock. The model's flow rate is computed by repeated simulation at varying turn proportions in Chapter 3. The flow-vs-turn-proportion expressions are also estimated by applying a mean-field approximation to the model in Chapter 4. This approximation treats the velocity and density as not varying from cell to cell allowing a simplified analytical approach to estimating the flow rate. Finally, a video-based vehicle tracking application is used to measure the flow rate vs turn proportion in Chapter 5. The video tracking uses blob detection combined with Multiple Hypothesis Tracking [Reid 1979] to estimate vehicle locations and velocities. Using initial and final position, turns are detected. By recording the turn decision and reprocessing the video, the flow-vs-turn proportion can be calculated at each frame. The resulting empirical data is compared with simulated and analytical results in Chapter 6. The proportion of left-turning traffic is universally found to have a strong negative effect on traffic flow. The simulation and mean-field approximations give similar results but the approximation tends to underestimate flow at low proportions of left-turning traffic and high proportions of right-turning traffic. The measured flow rate shows a weak positive relationship with the proportion of nonturning

traffic and no clear relationship with the proportion of right-turning traffic.

1.1 Traffic models

A common goal of traffic models is to describe flow in terms of other variables. Most often, the flow is taken to be a function of density; the function giving flow in terms of density is know as the *fundamental diagram*. Figure 1.1 is taken from a signalised intersection but shares some characteristics with the fundamental diagram of highway traffic. At low densities, traffic is nearly free to travel at its maximum velocity and flow is approximately linear in density. At higher densities, decreased vehicle velocity causes a net decrease in traffic flow and a higher velocity variance.

One reason for the popularity of the cellular automata (CA) models is their ability to reproduce features of the flow-density measurements as in Figure 1.4. In particular, the CA models yield a higher slope in the low-density "free-flow" region and a lower, negative slope in the "congested" high-density region. The CA models also have a higher variance in the congested region as exhibited in Figure 1.1. The interpretation of the higher-variance downward segment of the fundamental diagram is a source of contention among traffic researchers [Brockfeld *et al.* 2008]. Kerner's [2004] "Three-phase theory" argues that the negatively sloped region in the fundamental diagram is composed of two separate phases. The existance and characterization of multiple phases is a major goal of many traffic models [Levine *et al.* 2004, Farhi *et al.* 2011].

The development of traffic models has generally been in the direction of increasing discretization in order to facilitate simulation. Early partial differential equation-based models were continuous in density, position and time. These macroscopic models share similarities with

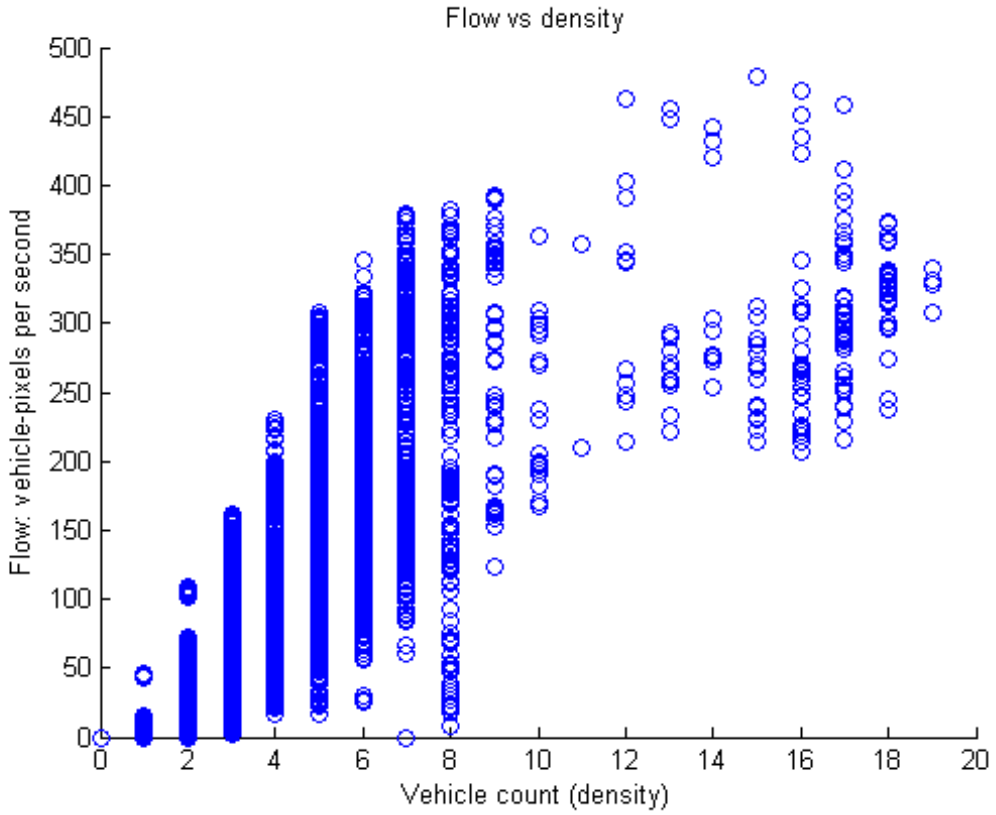

Figure 1.1: Fundamental diagram, Harbord St. & Huron St., Toronto, Ontario

the Navier-Stokes equations [Kerner & Konhhauser 1993, Velasco & Marques 2005]. Daganzo [1995] criticizes fluid dynamic models for exhibiting backward flow in some situations due to the anisotropic (directionally asymmetric) nature of fluid in contrast to the forward/reverse asymmetry of traffic.

A class of models based on cellular automata [Nagel & Schreckenberg 1992] allow representation of anisotropic particles. Cellular automata are discretized in space and time which facilitates fast simulation. Petri net-based traffic models [Farhi *et al.* 2009] use a similarly discretized representation with the additional capability of allowing asynchronous, local state transitions. In contrast, cellular automata follow a parallel update procedure in which all cells undergo state transitions simultaneously.

1.1.1 Lighthill-Whitham Model

Lighthill & Whitham [1955] described the propagation of density waves on long roads using a partial differential equation (PDE) in density and position. No attempt was made at theoretically deriving a relationship between flow and density; the authors assume only that flow is a function of density. This assumption combined with continuity conditions on traffic density allows the authors to derive the propagation speed of density waves along highways. The PDE could be discretized for simulation but it would still retain its difficiencies: symmetrical dynamics, an unspecified flow-density relationship and no apparent method of incorporating turning rules. Lighthill and Whitham discuss the impact of periodic red and green lights on a traffic stream. An approximation is given for flow capacity as a function of light timing. The propagation of shock waves caused by the green-red transition is discussed. No vehicles are assumed to turn left or right at a junction. The resulting analysis provides an explanation of queue growth at intersection as a function of total intersection capacity. The location of the "shock wave" (discontinuous density) is traced as a red light turns green. When the intersection is operating below the maximum flow capacity, the shock wave will travel through the intersection during a green light.

1.1.2 Gas Kinetic models

Prigogine & Andrews [1960] used a particle physics-based integral differential equation derived in a manner similar to the Boltzmann equation for the time evolution of particle density distribution functions. A version of the Lighthill-Whitham equations with an added diffusive term can be derived from Prigogine's gas kinetic models [Helbing 1996].

1.1.3 Car following models

Chandler *et al.*'s [1958] "car following model" describe the movement of chains of vehicles on a long highway as a function of the gp ahead. Acceleration is considered to be a function

of gap size. Herman *et al.* [1959] perform stability analysis on chains of vehicles all following the same gap-based feedback law.

1.1.4 Petri nets

Petri nets and hybrid petri nets (combining discretized with continuous states) [Di Febbraro & Sacone 1998] have been applied to investigate unified models of transportation networks including roads, junctions and control devices. The state and transition rules are discretized; in some models the transitions are stochastic . Petri nets are capable of representing multiple asynchronous processes. Graphical representations of Petri nets allow some correspondence with the geometric aspect of transportation systems.

1.1.5 Cellular automata and TASEP

Von Neumann [1966] first introduced the notion of cellular automata (CA), systems discretized in position, state and time. Elementary CA follow local transition rules; the next state of each cell is a function of the cell's current state and the state of adjacent cells. Nonelementary CA use transition rules which may be a function of some local neighbourhood. Navier-Stokes equations can be derived from CA models under a wide variety of model assumptions [Wolfram 1986]. In addition, CA have been studied as models of traffic. In particular, a simple one-dimensional CA known as Wolfram rule 184 is the basis for many traffic models. The state of each cell is binary (interpreted in traffic models as being either occupied or unoccupied by a vehicle). A lane is represented as a one-dimensional lattice with a cell at each site. The rule's name is derived from the elements of its state transitions table (Table 1.1) [Wolfram 2012] by converting to base-10 representation. Each cell's next state is a function of its own state and that of the adjacent cells. The upper row in Table 1.1 enumerates all possible three-cell state combinations. The bottom row indicates the state of the middle cell after one time step. Put simply, an occupied cell moves to the right if possible. Otherwise, it does not move. This is a CA version of a transport process. A model

known as the "asymmetrical simple exclusion process" (ASEP) is closely related to rule 184; the standard ASEP allows particles to move in either direction with some probability. The totally asymmetrical simple exclusion process (TASEP) requires particles to move in only one direction. In contrast to rule 184, each lattice site is updated asynchronously in the TASEP.

Table 1.1: Rule 184 state transitions

Current state	111	110	101	100	011	010	001	000
Next state	1	0	1	1	1	0	0	0

Figure 1.2 illustrates the behaviour of an 8-segment road initialized with only a single cell occupied.

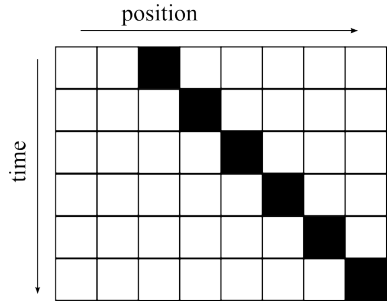

Figure 1.2: Rule 184 example

1.1.6 Nagel-Schreckenberg model

Nagel & Schreckenberg [1992] extended the rule 184 CA with two additions. First, occupied cells ("vehicles") can now move with an integer speed v_{max} instead of only one cell per timestep. Second, a randomized braking step is introduced: In addition to braking to avoid collisions, vehicles now also decelerate one unit randomly with probability p. The road is toroidal, therefore the model is translation invariant; all cells are connected in the same manner. The state transition rules of this model—the NaSch model for short—are given in detail below. The i^{th} vehicle's velocity at timestep k, $v_i(k)$ is updated once per timestep according to the following rules. The headway (distance to next vehicle) for vehicle i is

written h_i.

1. $v_i(k + 1/4) = \min(v_{max}, v_i(k) + 1)$
2. $v_i(k + 2/4) = \min(h(i), v_i(k + 1/4))$
3. With probability p, $v_i(k + 3/4) = \max(v_i(k + 2/4) - 1, 0)$ otherwise $v_i(k + 3/4) = v_i(k + 2/4)$
4. Advance each vehicle by v sites

Acceleration and braking are asymmetrical; the vehicles can only accelerate by one unit per timestep while braking can occur at any rate up to v_{max} per timestep. This acceleration-deceleration asymmetry is reflected in its fundamental diagram (Figure 1.4). Note that the slope of the initial segment (increasing flow with density) is steeper than the slope of the decreasing segment. This is shown experimentally using Monte Carlo simulations [Nagel & Schreckenberg 1992] and analytically using mean-field approximations in [Schreckenberg *et al.* 1995].

Figure 1.3 shows a series of initial and final states after one timestep with $v_{max} = 1$. The first sequence illustrates a vehicle moving forward; this occurs with probability p. The second sequence illustrates the random-braking rule; this occurs with probability $(1 - p)$. The third sequence illustrates the collision braking rule; cars do not move forward if a collision would result. The fourth sequence illustrates unimpeded movement: no collisions can occur at time $k = 2$ and the probabilistic braking has not occured so all vehicles move forward.

An important feature of this model is its fundamental diagram for two reasons. First, it reflects the asymmetry observed in real traffic flow-density curves. Second, it reflects the increased flow variance at high density. The asymmetry in the positive and negative slopes of the flow curve is a result of the asymmetrical acceleration and braking rules; it is possible to decelerate at any rate up to v_{max} per timestep while vehicles may only accelerate by one

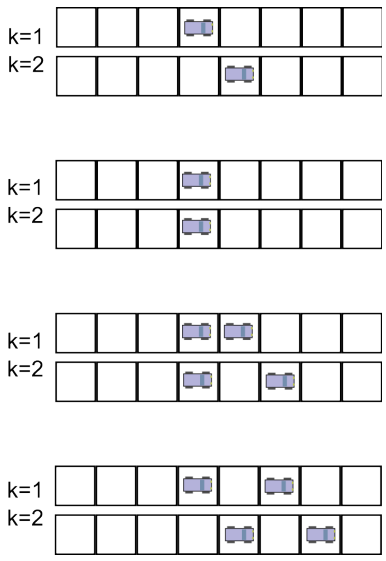

Figure 1.3: State transition illustrations

unit per timestep. The increased variance of the flow rate at higher densities is caused by the random braking. When the braking probability is set to zero, no variance in flow rate (from run to run) at higher densities is observed. At $v_{max} = 1$ and $p = 0$ the NaSch model degenerates to rule 184.

The boundary conditions in the NaSch model are usually taken to be toroidal. This means that if a vehicle is at site i moving at velocity v such that $i + V > N$ where N is the length of a lane, the vehicle's destination site will be $i + V - N$. This justifies the assumption that the traffic density c and other statistics are equal for each cell because the lattice index can be shifted without affecting the dynamics.

1.1.6.1 Mapping CA model state to macroscopic variables and measurements

Formally, the macroscopic density variable c is given by:

$$c = \frac{\sum_{i=1}^{N} \delta_i}{N} \tag{1.1}$$

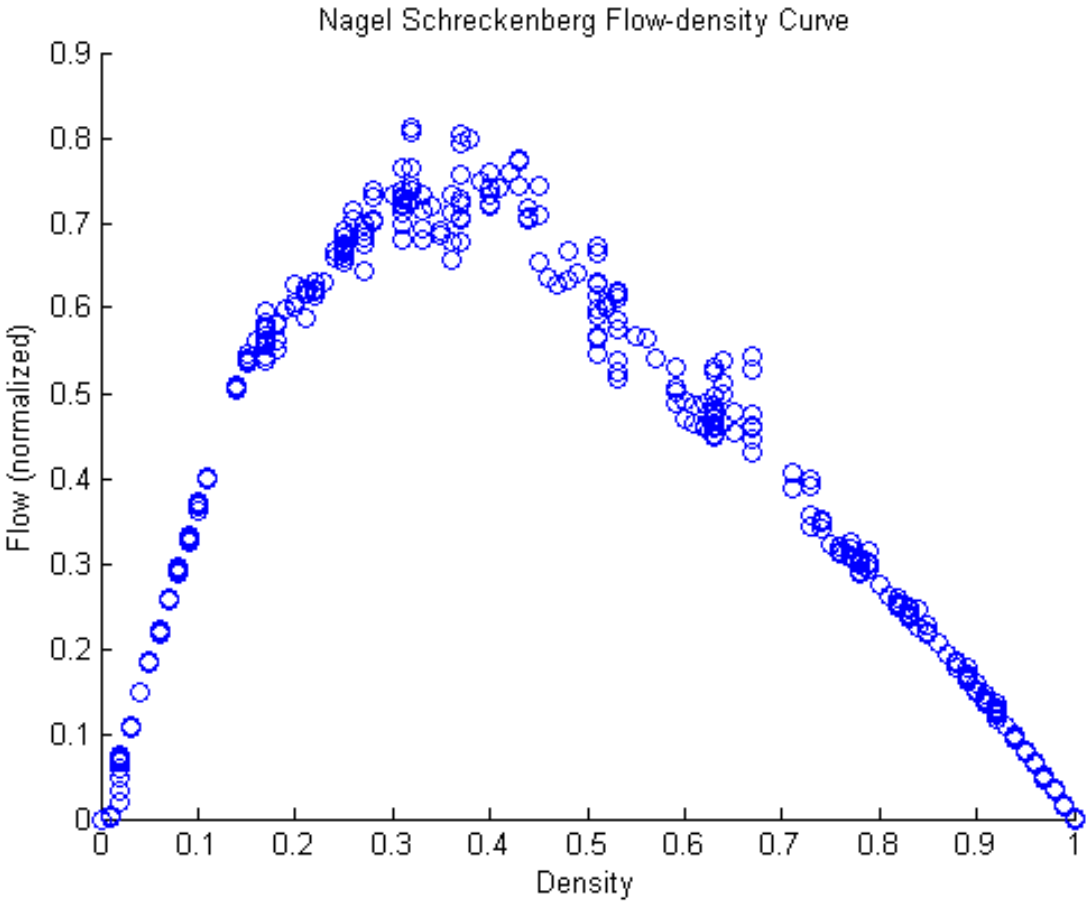

Figure 1.4: Simulated NaSch flow density curve

where N is the number of cells in a lane and δ_i is an indicator variable:

$$\delta_i = \begin{cases} 0 \text{ if cell } i \text{ is unoccupied} \\ 1 \text{ otherwise} \end{cases} \tag{1.2}$$

The average velocity v_{avg} is given by

$$v_{avg} = \frac{\sum_{i=1}^{N} v_i}{\sum_{i=1}^{N} \delta_i} \tag{1.3}$$

where

$$v_i = \begin{cases} \text{velocity of vehicle } i \text{ if } \delta_i = 1 \\ 0 \text{ otherwise} \end{cases} \tag{1.4}$$

The net flow is then given by

$$J = v_{avg} c \tag{1.5}$$

The left-turn proportion variable L is given by

$$L = \frac{\sum_{i=1}^{N} L_i}{\sum_{i=1}^{N} \delta_i} \tag{1.6}$$

where

$$L_i = \begin{cases} 1 \text{ if cell } i \text{ is occupied by a left-turning vehicle} \\ 0 \text{ otherwise} \end{cases} \tag{1.7}$$

and similar expressions give the right turn proportion R and straight-through proportion T.

Individual cells are normally considered to represent a distance of 7.5 m based on the amount of area a single vehicle occupies in a complete jam [Nagel & Schreckenberg 1992]. Allowing free traffic (at $v_{max} = 5$) to map to 120 km/h results in one timestep representing approximately 1 second. The slowest speed (1 cell per timestep) maps to 24 km/h.

1.1.7 Traffic model summary

The trend in traffic modeling appears to be in the direction of microscopic simulation. Systems based on CA have been implemented to simulate large networks in real time [Esser & Schreckenberg 1997]. Extensions to CA-based traffic models encapsulate a wide variety of phenomena (multilane traffic [Kanai 2010], jamming in bus routes [O'Loan *et al.* 1998]). The ease of stating rules programmatically is an attractive feature of CA-based models. Consider the systems of integral/differential equations that would be necessary to state the rules of traffic at an intersection in a Lighthill-Whitham or car-following model. Although possible,

it is more intuitive to state rules of traffic in discretized form. Both Petri nets and CA allow discretized rules. These two approaches share many similarities; their technical differences do not significantly distinguish their ability to represent traffic phenomena. It appears that CA are becoming the framework of choice for statistical models of traffic based on recent literature reviews [Chowdhury *et al.* 2000, Maerivoet & De Moor 2008].

Table 1.2: Traffic models

Type	Symmetrical particles	Macroscopic	Continuous
Kinematic wave	yes	yes	yes
Boltzmann gas	no	no	no
Car following	no	no	yes
Petri net	no	no	no
Cellular automata	no	no	no

Table 1.2 summarizes the most well known models for single-lane traffic.

1.2 Existing intersection models and extensions to the Nagel-Schreckenberg model

Various intersections models based on cellular automata have been proposed. In several cases, the models are used to study multi-intersection dynamics. Simplified models allow a user some control over flow rate variables but often do not accurately represent the interactions of the traffic within the intersection. Often only a subset of normal manoeuvres/turn decisions are available.

1.2.1 Biham-Middleton-Levine model

The Biham-Middleton-Levine (BML) model [Biham *et al.* 1992] was an early description of two-dimensional traffic flow; this was not an attempt at describing intersections in a geometrically realistic manner but an attempt at studying jamming as a two-dimensional phase change. The BML cells are located on a two-dimensional lattice; each cell represents a

sort of intersection. Cars do not turn in intersections, they only wait for conflicting vehicles to pass. This model can be thought of as the limiting approximation where some area is composed entirely of intersections with zero-length roads and vehicles always pass straight through each intersection heading either north or east. Figure 1.5 illustrates the BML model with vehicles travelling either north or east. The BML model can be considered to be a two-dimensional analogue of rule 184.

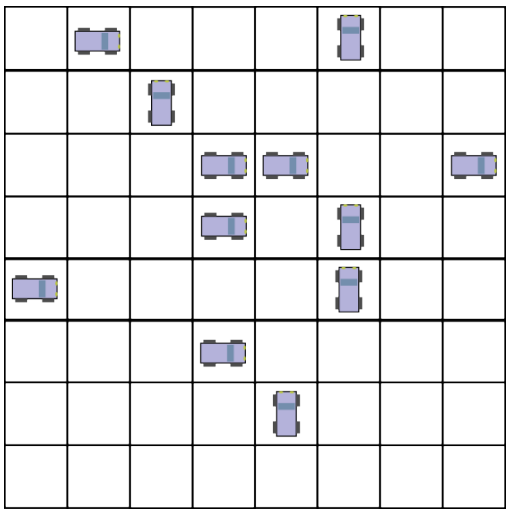

Figure 1.5: Biham-Middleton-Levine model

1.2.2 TASEP with crossing

Nagatani [1993] extended the totally asymmetric simple exclusion process (TASEP) to systems with a crossing of two one-dimesional lattices (Figure 1.6). Dependence of flow on particle (traffic) density is investigated. Shock formation resulting from the crossing is compared with shocks resulting from a "collision." Dynamic phase transitions are found to occur successively with increasing density. Nagatani states that the results are the same using parallel or random sequential site updates. This model can be interpreted as an unsignalised intersection; the only reason a vehicle would not enter the intersection is occupation by another vehicle.

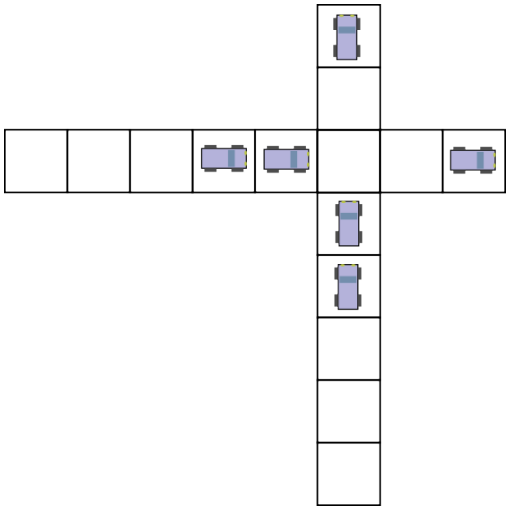

Figure 1.6: TASEP with crossing

1.2.3 Unsignalised intersections

Ruskin & Wang [2002] describe a cellular-automaton model for unsignalised intersections. This model extends the TASEP intersection by allowing integer speeds and allowing turning from a single-lane minor (smaller) road to the two-lane major road. The effect of variation in gap size for which a driver is willing to enter a conflicting stream is investigated. Model flow rates are calculated with varying driver decision strategies and varying turn proportions. The characters inside cells in Figure 1.7 describe the rules allowing a vehicle at the stop sign to enter the intersection. For the vehicle at the stop sign to enter, cells marked *0* must be unoccupied; cells marked *a* must be either vacant or occupied by right-turning vehicles; cells marked *b* must not be occupied by a right-turning vehicle. In the signalised intersection model described in Chapter 2, similar rules are employed where a vehicle is allowed to proceed dependant on the turn decisions of vehicles in nearby cells. Figure 1.7 illustrates the cells whose occupation states are checked when a vehicle at the minor (northbound) approach attempts to enter the intersection.

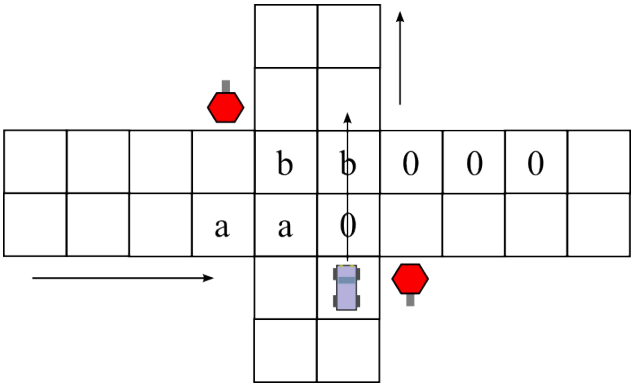

Figure 1.7: Unsignalised Intersection

1.2.4 Rotary (Chopard) model

Chopard *et al.* [1996] describes an intersection model (Figure 1.8 in which cars enter the intersection giving priority to vehicles already in the intersection and vehicle exiting is controlled by a binary flag, the value of which is not specified by the model. This allows an implementation to mimic the characteristics of various intersection types; for instance, the flag can be randomly selected or switched periodically to imitate a signalised intersection. For this reason, the Chopard model may be a useful predictive tool for networks larger than a single intersection. However, the model is not predictive of flow rates at the intersection level; these are manually specified by the user.

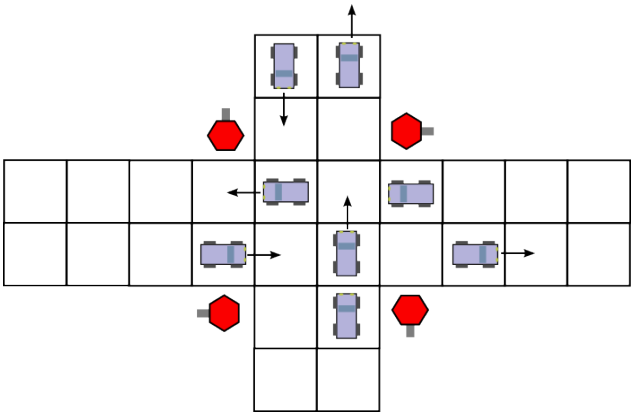

Figure 1.8: Chopard model

1.2.5 Dallas intersection

Rickert & Nagel [1997] describe a microsimulation of multilane intersections (Figure 1.9) in the the Dallas/Fort Worth area which treat vehicles as jumping across the intersection, never occupying common cells. This effect is pointed out and a suggested workaround is to introduce an additional braking probability at the transfer points. This strategy suffers from the same problem as the Chopard model in the sense that it may be a useful tool for studying larger networks of intersections but it does not explain intersection-level flow rates; it provides a model to generate a given flow rate. A similar criticism is that this strategy requires introduction of additional variables which should (or could) be produced by a model instead.

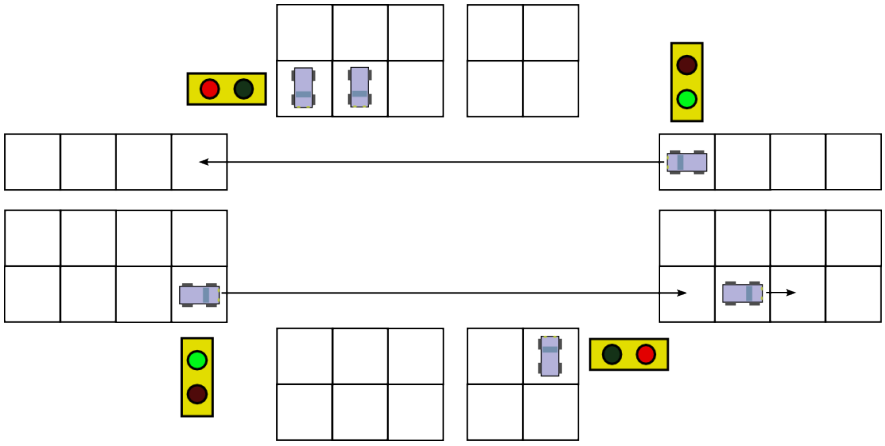

Figure 1.9: Dallas intersection

1.2.6 Signalised two-road NaSch model

Foulaadvand & Belbaasi [2008] introduce a model of a signalised intersection with two roads, one travelling north and one travelling east (Figure 1.10). This model describes the effect of a traffic light on straight-through traffic but does not allow turning vehicles. The authors consider the effects of various signal timing strategies on flow rate. Foulaadvand & Belbasi [2011] investigates an extension allowing turning.

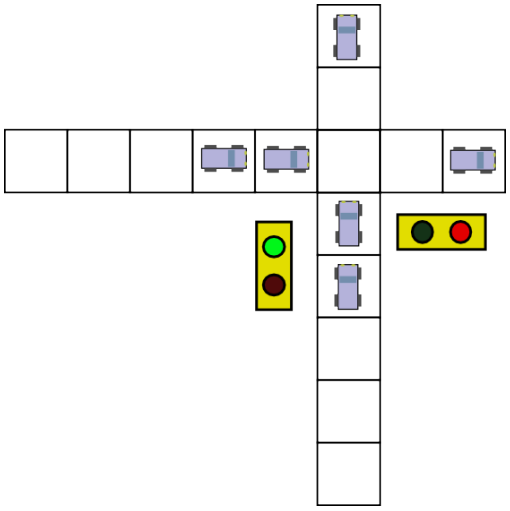

Figure 1.10: Foulaadvand Belbaasi model

1.2.7 Tonguz-Viriyasitavat-Bai model

A recent example [Tonguz *et al.* 2009] (TVB model) describes a four-way signalised intersection model in pseudocode. Like other CA-based intersection models, the TVB model uses the NaSch model roads plus additional rules at the intersection. The pseudocode does not fully specify some aspects of the simulation. In particular, vehicles are said not to move if the destination street is congested but no precise definition of this term is presented in context. In addition, vehicles are said to travel to the "destination street" upon certain conditions being satisfied; this seems to imply that the vehicles do not actually occupy the intersection center. This would eliminate the possibility of gridlock occuring. However, Figure 1 in Tonguz *et al.* [2009] shows vehicles apparently occupying the intersection centers.

1.2.8 Freund Pöschel model

Freund & Pöschel [1995] introduce another CA-based model for an unsignalised intersection. Every cell in a two-dimensional lattice is considered to be a four-way intersection, similar to the BML model. As in previous models, the vehicles do not occupy the center of the intersection; they jump from approach queue to destination lane. The effects of global

velocity on average vehicle density are investigated.

1.2.9 Rosenblueth-Gershenson model

Rosenblueth & Gershenson [2011] introduce a two-lane signalised intersection model capable of representing many of the features of a signalised four-lane intersection with the obvious exception of using two lanes instead of four. The potential for gridlock is eliminated when only two lanes intersect, simplifying the rules significantly. The requirement of preventing collisions is also simplified in the case of only two lanes.

1.2.10 Intersection travel time model

Lawniczak & Di Stefano [2009] present a model used for simulating total travel time through a series of roads and intersections. This intersection model is similar to the Dallas intersection in which vehicles jump from the end of one NaSch lane to the start of another lane. The rules vehicles obey when crossing intersections are not specified.

1.2.11 Intersection model summary

Table 1.3: Intersection models

Type	signalised	Four lane	Conflicting turns	Inner geometry
Kinematic wave	yes	no	no	no
BML	no	no	yes	no
Nagatani	no	no	yes	yes
Chopard	yes	yes	yes	yes
Ruskin & Wang	no	yes	yes	yes
Rickert & Nagel	yes	yes	no	no
Foulaadvand & Belbaasi	yes	no	no	yes
Rickert & Nagel	yes	yes	no	no
TVB	yes	yes	yes	no
Freund & Pöschel	no	yes	yes	no
Rosenblueth & Gershenson	yes	no	no	yes
Lawniczak	yes	yes	no	no

All of the above models (with the exception of the kinematic wave extension) are variations on two-dimensional analogs of rule 184 or the TASEP. The BML model intuitively seems to reflect a city composed of one-way lanes better than a single intersection. Nagatani's model appears to be the earliest model of a single intersection connecting two one-dimensional lanes. The effects of traffic density and signal timing on intersection networks have been investigated by several authors [Schadschneider *et al.* 1999, Kanai 2010]. The effect of turn proportion on flow rate has not been investigated to the author's knowledge. Chopard *et al.* [1996] notes that gridlock may occur in the rotary model if vehicles are not allowed to reroute. This type of gridlock occurs within a single intersection as in Figure 1.11; an intersection fully occupied by any combination of these turn choices will result in a permanent deadlock. Chopard's solution is to allow vehicles to reroute. Another way of addressing gridlock is to specify rules which prevent the gridlock-causing configurations from occuring.

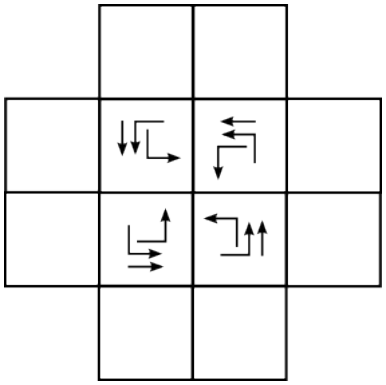

Figure 1.11: Gridlock permutations

The problem of specifying the rules for an intersection model can be broken down into two subproblems; maintaining flow and avoiding collisions. The following chapter details a set of rules which achieve these goals and allow all movements at a standard four-way intersection: left & right turns, and through traffic. Each vehicle passes through cells of perpendicular lanes that it crosses.

Chapter 2

Proposed Intersection Model

This chapter describes an arrangement of four single lanes (called northbound, southbound, eastbound and westbound) based on the Nagel-Schreckenberg model, illustrated in Figure 2.1. Each road follows approximately the same rules as the NaSch model. Vehicles near the intersection follow modified rules: in addition to the reasons for braking under NaSch dynamics (avoid collision with vehicle ahead and random braking), vehicles now brake to avoid collisions with vehicles in other lanes and to avoid gridlock.

A vehicle in the NaSch model will brake to avoid colliding with the vehicle ahead. Vehicles may not pass each other in a single lane; therefore, only rear-end collisions are possible. A NaSch vehicle on a single road only has to consider its own movements and the headway to the vehicle in front in order to avoid collisions. In an intersection, vehicles from separate lanes may be heading toward the same cell. Vehicles now must check whether vehicles in other lanes are headed toward the same cell and yield priority correctly if so.

The goal of preventing collisions is accomplished by restricting vehicle movements. The rules which restrict vehicle movements are only effective in specific situations. These rules are a function of location, the turn decision of the vehicle (left/right/non-turning), the location

and turn decisions of nearby vehicles and the state of the intersection light (red or green). The situations in which these rules apply are enumerated in detail below. A yellow light (assumed to mean that cars should stop if they possibly can) would be exactly equivalent to a red light if cars are modeled as being able to stop at any rate up to v_{max} per timestep. For this reason, yellow lights are not included in the model.

In addition to preventing collisions, traffic flow must be maintained. If vehicles' motion is restricted too much, no movement will occur. This can manifest itself in a variety of ways. If the priority level of conflicting traffic is undefined, neither vehicle may safely proceed; this would cause both vehicles to wait indefinitely. Gridlock may occur if vehicles enter into a situation in which no movement is possible. These situations must be prevented in addition to collisions. These situations are prevented through further restriction of vehicle movement so that vehicles may not proceed into gridlock.

Finally, some mechanism causing a vehicle to move from one lane to another is necessary. In the single-lane NaSch model, vehicles travel down their lane of origin. In the intersection, a turning vehicle has a lane of origin and destination. Upon arrival at the lane of destination, a vehicle must stop travelling in the original direction. This stopping is accomplished through an additional rule at the intersection. The vehicle then proceeds down the destination lane in the same manner as a vehicle in the single-lane model.

The rules each vehicle follows are designed to simulate a four-way signalised intersection. Left turns are allowed during green lights and right turns are allowed during both green and red lights. Left-turning vehicles move during the same phase as nonturning vehicles (green); they wait for suitable gaps in the oncoming traffic. Right turning vehicles behave similarly, only turning right during a red light if a gap in conflicting traffic is available. In addition to waiting for gaps before turning, vehicles follow additional rules. To avoid gridlock and

conflicts caused by ambiguous priority levels, vehicles will not enter the intersection under certain circumstances. Finally, right-turning traffic is obligated to stop at red lights before entering the destination lane.

The new rules are applied before random braking in the NaSch model. The distance each vehicle may travel before colliding with the vehicle ahead is called the headway (h_i for vehicle i) in the NaSch model. This intersection model extends the headway function h_i into a function g_i which gives the maximum distance a vehicle may travel before colliding or stopping due to an intersection rule. Let $r_1 ... r_6$ be the distance between a vehicle and the nearest site where intersection rule r in application, then the extended headway function g_i is now given as

$$g_i = \min(h_i, r_1 \dots r_6)$$

This distance is obtained by considering each cell in front of a vehicle i up to a distance of v_i cells ahead. The first cell which is currently subject to an intersection rule determines the safe distance. Following the calculation of safe distance, each vehicle may also brake randomly as in the NaSch model. The state transition rules for this intersection model are:

1. $v_i(k + 1/4) = \min(v_{max}, v_i(k) + 1)$
2. $v_i(k + 2/4) = \min(h(i), v_i(k + 1/4))$
3. With probability p, $v_i(k + 3/4) = \max(v_i(k + 2/4) - 1, 0)$ otherwise $v_i(k + 3/4) = v_i(k + 2/4)$
4. Advance each vehicle by v sites

The state is composed of:

- Location of each vehicle
- Velocity of each vehicle

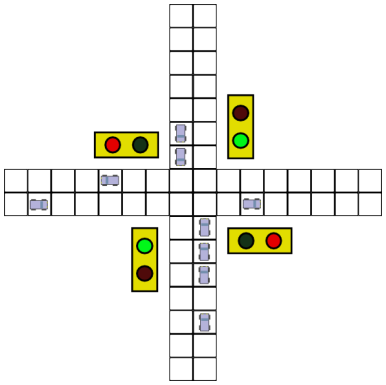

Figure 2.1: Signalised Intersection Model

- Turn decision of each vehicle
- Color of light

The static model parameters are:

- v_{max}: Maximum velocity, $v_{max} \in \mathbb{N}$
- p: Random braking probability, $0 \leq p \leq 1$
- a: Approach distance, $a \in \mathbb{N}$
- s: Signal split - percentage of time the signal is green , $0 \leq s \leq 1$
- L: Probability of a vehicle turning left, $0 \leq L \leq 1$
- R: Probability of a vehicle turning right, $0 \leq R \leq 1$
- T: Probability of a vehicle not turning, $0 \leq T \leq 1$
- $G_{N,S,E,W}$: Vehicle generation rate at the first cell in an approaching lane (Figure 2.2). Each rate may be set individually. A vehicle generation event occurs with probability G if the first cell in an approach is unoccupied. $0 \leq G \leq 1$
- $D_{N,S,E,W}$: Vehicle deletion rate at the last cell in an exiting lane. Each rate may be set individually. A vehicle deletion event occurs with probability D if a vehicle is about

to exit the intersection. If the event does not occur, the vehicle is prevented from travelling beyond the last cell in on the road. $0 \leq D \leq 1$

The turn proportions are constrained: $L + R + T = 1$. Vehicles are created in the first cell of each lane and deleted when they leave the final cell of their destination lane. The turn decision of each vehicle is initialized randomly with probabilities L, R, T when the vehicle is created. There are only two signal phases: red and green (no yellow light). This is because cars are treated as being able to decelerate from v_{max} to 0 in one timestep. In this situation, vehicles would treat yellow lights the same as red lights.

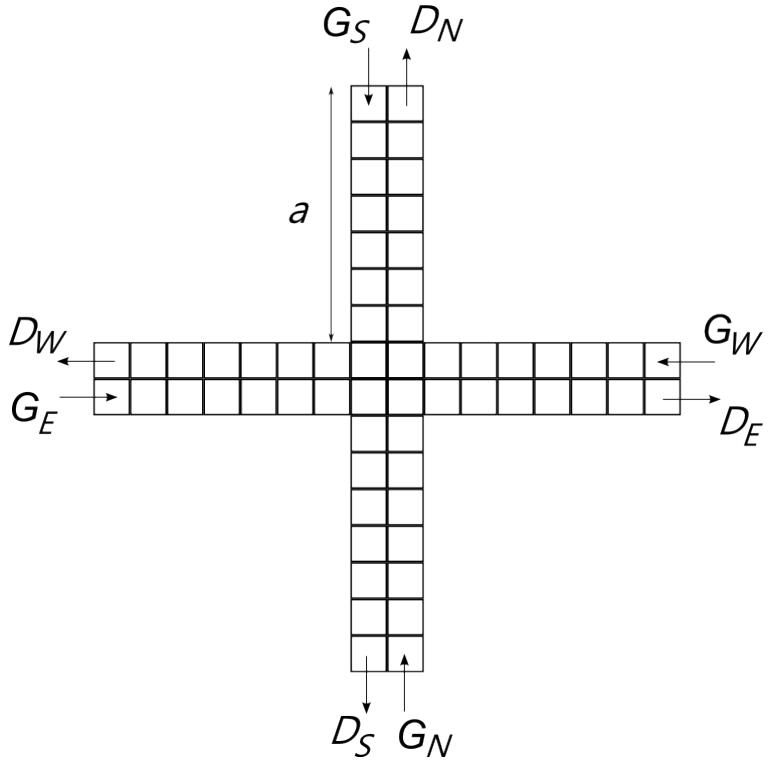

Figure 2.2: Static Intersection Parameters

The additional rules active near the intersection can be summarized:

1. Brake if the vehicle under consideration must yield to higher-priority traffic
2. Brake if arriving at red light
3. Brake if light is red and vehicle is travelling straight or turning left

4. Brake to prevent turning traffic from overshooting destination lane

5. Brake if a conflict could result from ambiguous priority

6. Brake if entering the intersection risks gridlock

For a vehicle moving in any cell, the applicability of each rule is checked at each timestep. The intersection-specific rules (1-6) do not apply along the entire lane. The maximum distance at which a vehicle may still be subject to intersection-specific rules is v_{max}; for example, if a vehicle is headed towards an intersection during a red light at distance of v_{max} cells and speed v_{max} cells per timestep, braking will be required under rule (2). Thus the region of intersection-specific rule application is larger for intersections with a higher v_{max}. In the case $v_{max} = 1$ (used here), the total region in which intersection-related rules apply is only three cells per lane. This includes the cell immediately before the intersection and the two cells inside the intersection. Each rule applies on a different subset of these cells. The factors dictating the applicability of each rule are detailed below. The rules for each lane are the same. They are described below from the perspective of northbound traffic.

2.1 Rule (1): High priority

Rule (1) represents the notion of waiting for higher-priority traffic to pass. In this context, high-priority traffic means nonturning or left-turning vehicles travelling forward during a green light. The trajectory of high priority traffic is calculated for the next timestep; these cells are "marked" by the high-priority traffic. Lower-priority traffic is prevented from moving to or through a cell marked by high-priority traffic. Left-turning vehicles are only considered to be high-priority in their initial direction of travel. This causes left-turning traffic to wait for nonturning vehicles before proceeding in the direction of the destination lane. Since left-turning traffic does not mark its trajectory when exiting the intersection in its destination lane, an additional rule (5) is necessary to prevent it from colliding with right-turning traffic

entering the intersection.

Low-priority vehicles are blocked by the trajectory of high-priority traffic (indicated by grey squares) in Figure 2.3.

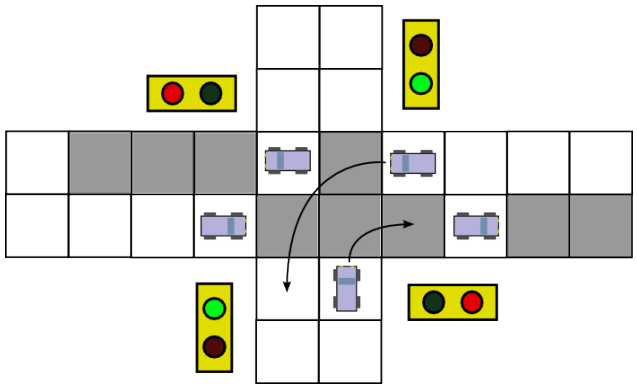

Figure 2.3: Yielding to high priority

2.2 Rules (2) and (3): Red lights

Rule (2) causes right-turning traffic to stop upon arrival at a red light. In conjunction, rules (2) and (3) allow right-turning traffic to turn during a red light after stopping while blocking left-turning and straight-through traffic. It may seem that one rule would be sufficient to enforce stopping at a red light. However, the fact that right-turning traffic is allowed to proceed after stopping differentiates this situation from left and nonturning traffic which must remain stopped at the red light. Figure 2.4 illustrates the requirement for a right-turning vehicle to stop before turning right; the vehicle must be moving, turning right and the light must be red. Figure 2.5 illustrates the distinct rule which causes left and nonturning traffic to remain stopped.

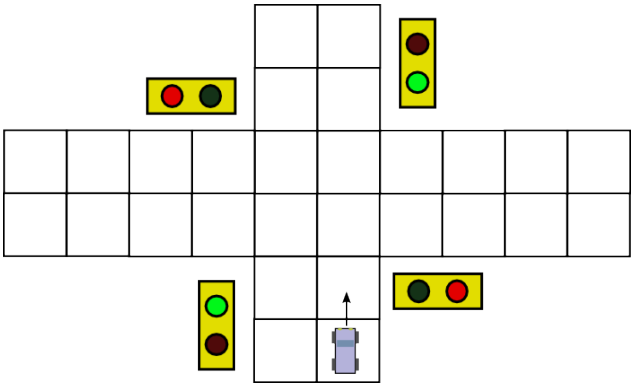

Figure 2.4: Stopping at red light

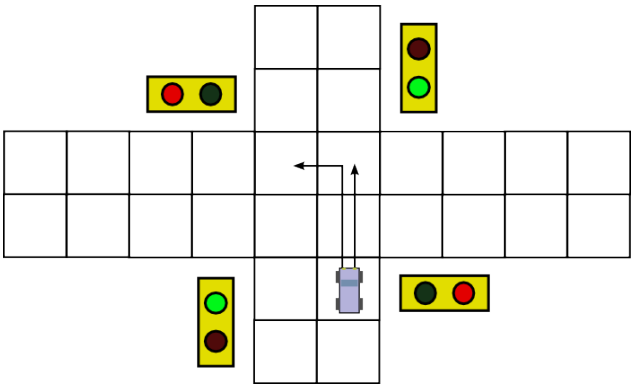

Figure 2.5: Waiting at red light

2.3 Rule (4): Turning

Rule (4) prevents traffic from travelling down its original lane once the destination has been reached. The rules are applied for each lane individually; the turning rule does not activate when the vehicle is travelling in the direction of the destination lane and so the traffic exits the intersection. Figure 2.6 illustrates vehicles travelling northbound, stopping to turn left or right. The vehicles are only considered to be stopped in one dimension (north/south); they are free to move down the destination lanes (east/west).

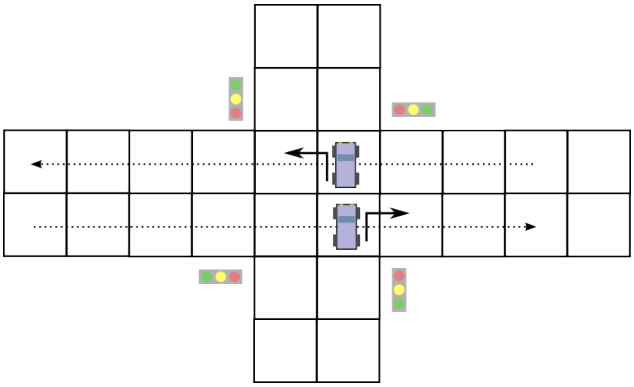

Figure 2.6: Stopping to turn

2.4 Rule (5): Late occupation

Rule (5) prevents right-turning vehicles from entering the intersection if the near-left corner is occupied by a left-turning or straight-through vehicle heading toward the right-turning vehicle, illustrated in Figure 2.7. Under normal circumstances, a vehicle turning left from the eastbound lane would normally not occupy this position while the northbound lane has a green light. However, it is possible; because of the random braking rule, a vehicle could potentially stop in any cell it occupies indefinitely. For this reason, the case of vehicles left over from previous signal phases still occupying the intersection must be considered.

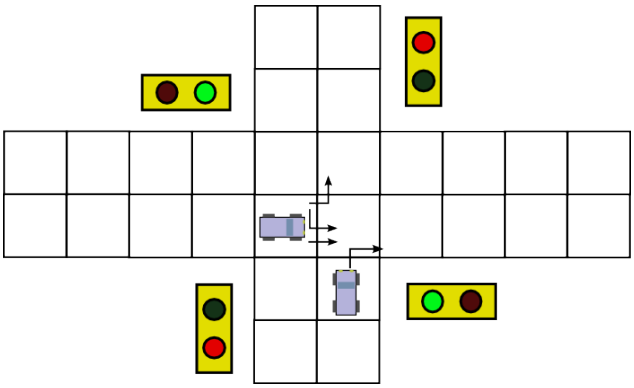

Figure 2.7: Intersection occupied

2.5 Rule (6): Gridlock

The purpose of Rule (6) is to prevent gridlock. Figure 2.8 illustrates a car stopping outside the intersection in order to prevent gridlock (as in Figure 1.11) from occuring. In the formulation of anti-gridlock rules, the Nagel-Schreckenberg model's randomized braking rule plays an important role. Any vehicle could remain stopped with nonzero probability for an unlimited amount of time. Therefore any cell may contain a vehicle which entered in a previous light phase. Vehicles entering the intersection need to deal with these "left-over" vehicles from a previous phase.

Without Rule (6), long simulation runs with any left-turning traffic eventually reach gridlock. As noted by Chopard *et al.* [1996], this can be considered a metastable phase in which a normal flow-density curve exists until gridlock occurs. The Chopard model deals with gridlock by allowing vehicles to reroute; in fact, each vehicle has no inherent turn choice and simply exits on the intersection probabilistically. No such rule is necessary for models which do not include cells inside the intersection because gridlock cannot occur.

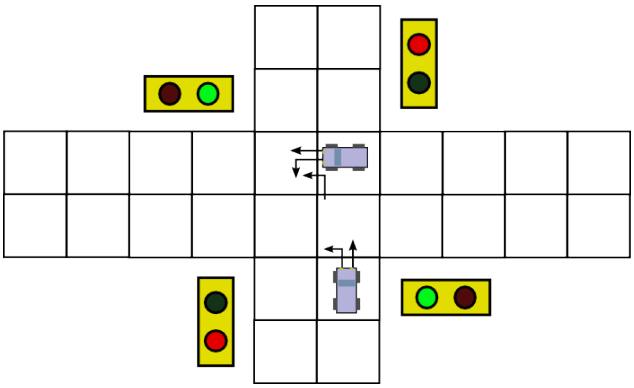

Figure 2.8: Gridlock

Chapter 3

Simulation

The intersection model is studied empirically by running the model under varying parameters while sampling the macroscopic model states (density c, velocity v_{avg}, turn proportions L, R, T). The results of simulating a single NaSch lane are presented first to provide a source for comparision for the intersection simulation results. Single-run simulations are compared against ensemble-averaged (Monte Carlo) simulations.

3.1 Implementation details

Both the road and intersection models are implemented as MATLAB scripts. A "single run" of a model occurs over a fixed number n of timesteps ($k = 1$ to $k = n$). The NaSch model is toroidal, therefore the total number of vehicles is conserved. In a single NaSch simulation run, the vehicles are all created at time $k = 1$. In contrast, the intersection model is nontoroidal with vehicles being created and deleted at first and last cells in each lane throughout the simulation.

3.1.1 Code Architecture

The intersection model simulation is structured like four normal NaSch roads run in parallel with the addition of intersection-specific rules at certain positions. These positions are

cells inside the intersection plus all cells up to a distance v_{max} from the intersection on the approach. State propagation is performed in two substeps at each iteration. The trajectory of high-velocity traffic is marked (the path of nonturning vehicles or left-turning vehicles in their original lane is projected forward for the next timestep to block lower priority traffic in the application of rule 1); then the allowed trajectories of lower-priority traffic can be calculated. The safe distance g_i is calculated for each vehicle. Following this, the normal NaSch dynamics are applied.

3.1.2 Sampling

Sampling the model's flow rates is done by an outer loop which set the intersection parameters, records macroscopic states and incrementally adjusts parameters every simulation run. The long-term average of macroscopic parameters (flow rates and densities) is recorded to sample the parameter-flow rate relationships.

3.2 Nagel-Schreckenberg simulation

The time-occupation plot of a single NaSch lane simulation run is illustrated in Figure 3.1. Black pixels represent vehicles/occupied cells. The vehicles travel to the right according to the NaSch rules detailed in Chapter 1. Backward-moving traffic jams are seen to emerge spontaneously as a result of the randomized braking step in the NaSch model. As the NaSch model is toroidal (vehicles leaving the last cell reappear at the first cell), the long-term statistics (density c, flow rate J) of each cell should be equal.

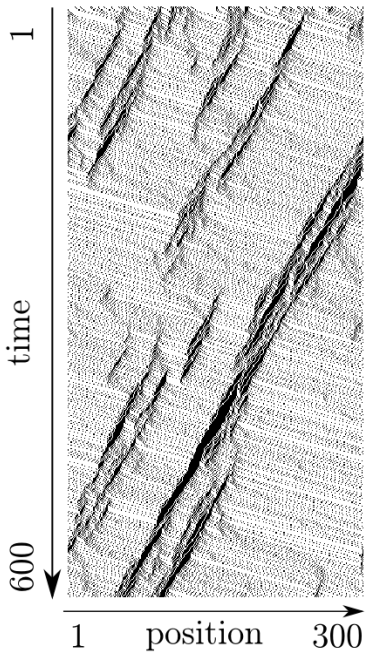

Figure 3.1: Single run of NaSch model

3.3 Intersection simulation

Each lane in the intersection model is sampled in the same manner as a single NaSch lane in Figure 3.1. Vehicles arrive at an equal rate in all directions and $L = 0.25, R = 0.25, T = 0.5$ for all lanes (that is, 25% of vehicles turn right, 25% turn left and 50% do not turn) in Figure 3.2. The intersection is at the midpoint of each lane. The periodic clusters of vehicles in the centre of each lane are queues forming at a red light. The queue formation on the northbound and southbound roads is offset by a 90° phase shift from queue formation on the eastbound and westbound roads. The vehicles in southbound and northbound roads travel in opposite directions (left to right and right to left respectively) as do the vehicles in westbound and eastbound directions.

Excluding the boundaries at the beginning and endpoint of each lane, the total number of

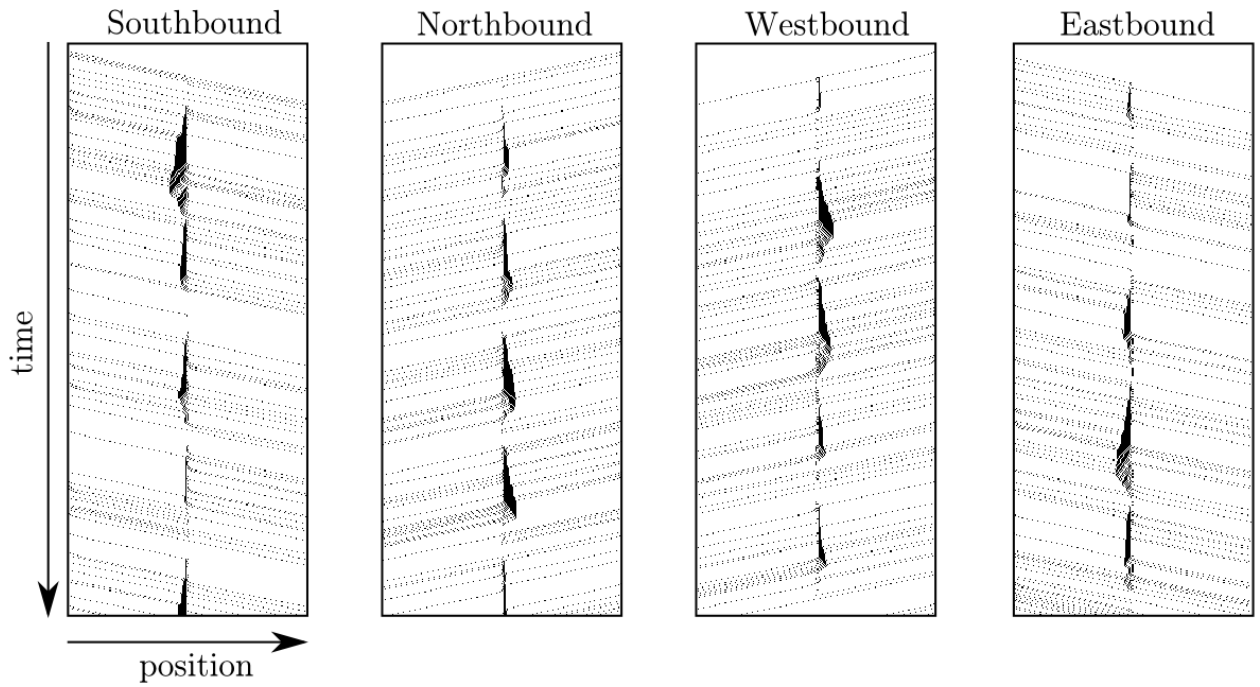

Figure 3.2: Single run of 4-way signalised intersection

vehicles is conserved. However, each lane is "nonconservative" considered on its own. This is illustrated in Figure 3.3 in which vehicles only arrive from the north and southbound lanes and only exit from the east and westbound lanes (all vehicles turn either left or right). In the north and southbound lanes, the intersection consumes (sinks) vehicles; in the east and westbound lanes, the intersection is a source.

Figure 3.4 illustrates the time-occupation plot of a single lane in an intersection averaged across runs. After averaging away the random influence of each individual run, the expected (most likely) component of the intersection state from run to run is obtained. The resulting density distribution is clearly position and time dependendent unlike a single NaSch lane. Figure 3.4 was averaged over 1000 runs of 150 timesteps each.

3.3.1 Steady-state assumptions

In calculating the flow rate, the intersection simulation is assumed to be in steady-state operation. The time required to reach steady state varies with approach length a and v_{max}.

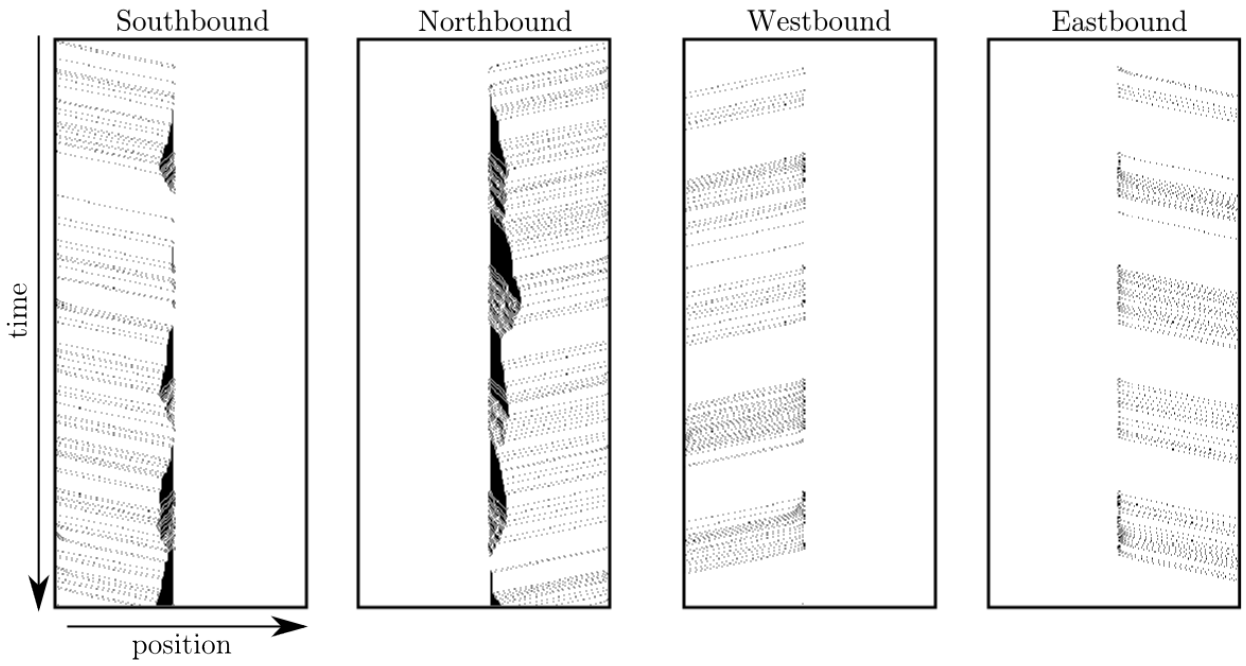

Figure 3.3: Signalised intersection, individual nonconservative lanes

Figure 3.5 shows Monte Carlo simulations of intersections with approach lengths $a = 40$ (left side) and $a = 250$ (three figures on the right side). The transient response time is increasing in a and nonmonotonic in v_{max} as indicated by the changes in response time as v_{max} is varied from 1 to 5 to 30.

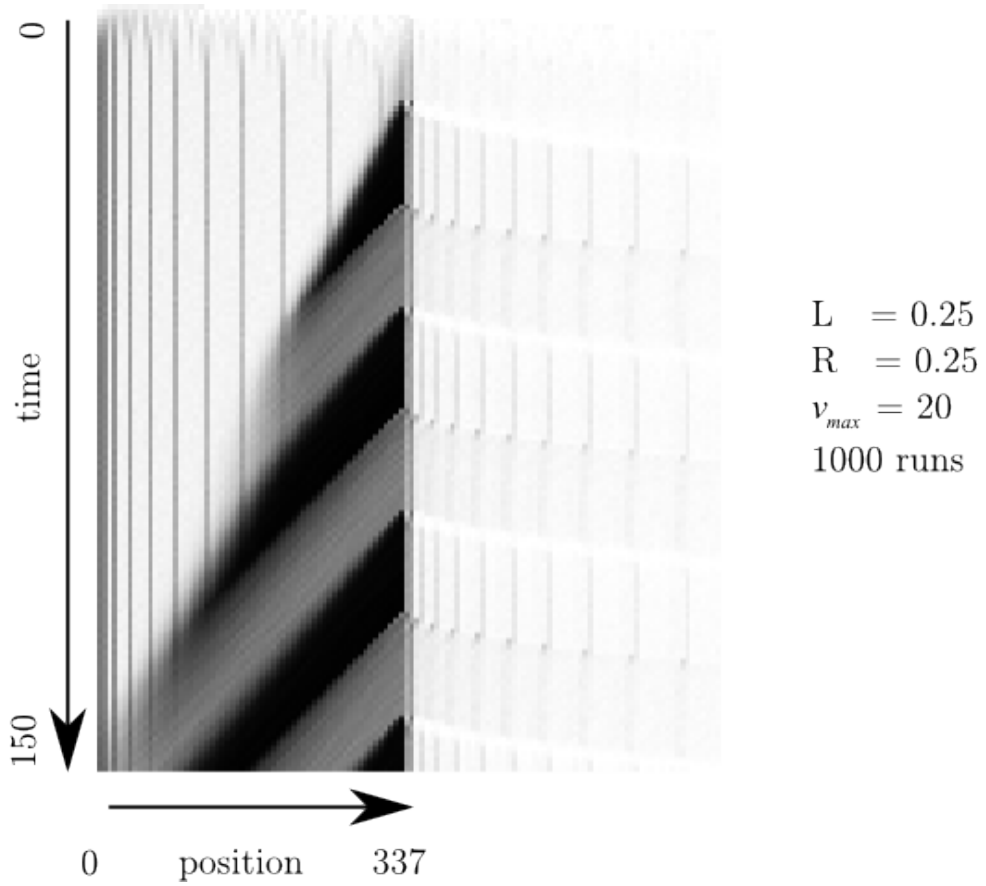

Figure 3.4: 1000-run average of intersection occupation

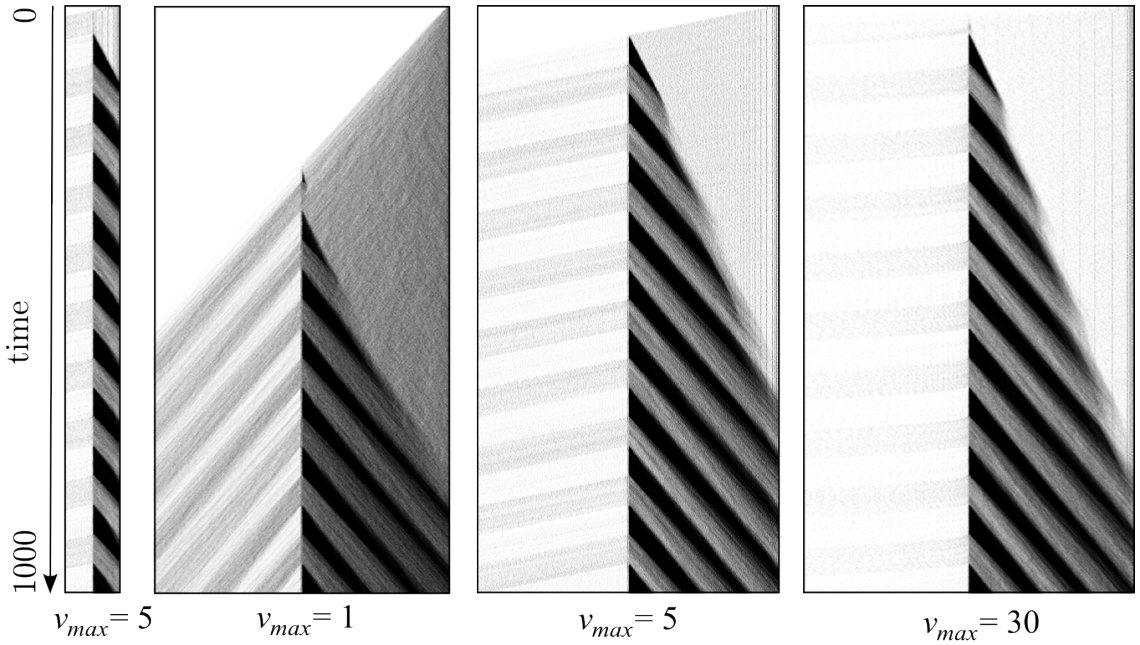

Figure 3.5: Transient response for various parameter settings

Chapter 4

Analytical Approximation

Mean-field approximations were used by Nagel & Schreckenberg [1992] to find analytical approximations to the fundamental diagrams of the single-road NaSch model. The average traffic flow rate in the intersection model of the previous chapter can be approximated analytically using similar assumptions.

All states of the model (density, velocity) are treated as probability distributions independent of position and time. This is illustrated graphically in Fig. 4.1. The update equation for the resulting probability distributions is formulated using the transition rules and the resulting linear equation is solved for the steady state density and velocity distributions.

4.1 Analytical approximation to the Nagel-Schreckenberg fundamental diagram

Schreckenberg *et al.* [1995] gives a description of the mean-field method as applied to the NaSch model in order to approximate the fundamental diagram (flow vs density relationship). The derivation is summarized here as the intersection is treated with the same method in the next section.

Consider a model with $v_{max} = 1$. The probability of a site i being unoccupied at timestep k

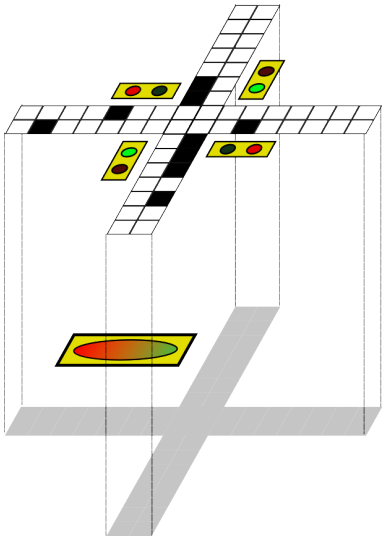

Figure 4.1: Graphical Illustration of Mean Field Approximation

is denoted as $d(i,k)$. The probability of a site being occupied by a vehicle of velocity zero is denoted $c_0(i,k)$ and the probability of a site being occupied by a vehicle of velocity one is denoted $c_1(i,k)$. The total probability of a site being occupied is denoted $c = c_0 + c_1$. The c and d distributions take into account all possible states for the model, therefore:

$$d(i,k) + c_0(i,k) + c_1(i,k) = 1 \tag{4.1}$$

The time is considered to take only integer values; $k+1/4, k+2/4, k+3/4$ can be considered stages in the calculation between k and $k+1$. After appling the NaSch acceleration rule, all vehicles accelerate by one step. This includes the stopped vehicles ($v_i = 0$). If $v_{max} = 1$, $v_i = 1$ for all vehicles. The probability distributions are given by

$$\begin{aligned} c_0(i, k+1/4) &= 0 \\ c_1(i, k+1/4) &= c_0(i,k) \end{aligned} \tag{4.2}$$

To avoid collisions, each vehicle must brake if the distance to the next vehicle is less than or equal to v_i. This can be thought of as the probability of a vehicle travelling at $v_i = 1$ times the probability of the next cell being occupied. The distributions after applying the collision

avoidance braking are

$$\begin{aligned} c_0(i, k+2/4) &= c_0(i, k+1/4) + c(i+1, k+1/4)c_1(i, k+1/4) \\ c_1(i, k+2/4) &= c_1(i, k+1/4)d(i+1, k+1/4) \end{aligned} \tag{4.3}$$

During the randomized braking rule, vehicles are randomly decelerated by one unit. This occurs with probability p for each vehicle at each timestep. After the randomization stage ($q = 1 - p$), the probability distributions are

$$\begin{aligned} c_0(i, k+3/4) &= c_0(i, k+2/4) + pc_1(i, k+2/4) \\ c_1(i, k+3/4) &= qc_1(i, k+2/4) \end{aligned} \tag{4.4}$$

Finally, after the movement stage the distributions are

$$\begin{aligned} c_0(i, k+1) &= c_0(i, k+3/4) \\ c_1(i, k+1) &= c_1(i-1, k+3/4) \end{aligned} \tag{4.5}$$

After removing dependence on time and position, the following update equations result:

$$\begin{aligned} c_0 &= (c + pd)c_0 + (1 + pd)cc_1 \\ c_1 &= qd(c_0 + c_1) \end{aligned} \tag{4.6}$$

Solving for c_0 and c_1,

$$\begin{aligned} c_0 &= c(c + pd) \\ c_1 &= qcd \end{aligned} \tag{4.7}$$

Since the total flow is given by c_1, this expression can be taken as an approximation to the fundamental diagram for the case $v_{max} = 1$. This approximation underestimates flow in the NaSch model when all cells are updated in parallel. The approximation becomes exact under random-sequential updates [Schadschneider & Schreckenberg 1998]. This is due to

short-range correlations between cell states under parallel update which do not exist under random-sequential update. In particular, an unoccupied space is more likely to appear in front of an occupied space than the mean field theory would predict under parallel dynamics. Because $d = c - 1$, it can be seen that c_1 is a negative quadratic in c (traffic density) and therefore yields a flow rate relationship like that in Figure 1.4. The asymmetry of Figure 1.4 is not present in Figure 4.7 as this solution only deals with $v_{max} = 1$. A derivation of the case where $v_{max} = 2$ yields an asymmetrical flow-density curve.

4.2 Mean-Field Approximation, from single-lane to intersection

In the single-lane case, the mean-field assumption of translation and time-invariant statistics is justified on the grounds that each cell really does obey the same laws across time and space. The probability distributions of vehicle density and velocity are equal everywhere. A time-occupation diagram averaged across enough runs would yield a uniform grey image. This is not the case for an intersection. Figure 4.2 illustrates the time and position independence of a single NaSch lane as compared to the time and position-dependent intersection lane. This decreases the validity of the mean-field approximation for intersections. Certain phenomena are not captured by a mean-field approximation; in particular, gridlock is not represented in the mean-field solution. This is because gridlock relies on a deterministic blocking effect; if gridlock occurs, it blocks the intersection completely. Under the mean-field approximation, gridlock only causes a statistical delay equal to the proportion of blocked vs unblocked cells. If, for example, the blocked cells (4 inner intersection cells) represent 10% of the total cells in the intersection, the mean-field approximation only sees a 10% chance of each vehicle being affected by gridlock in any position.

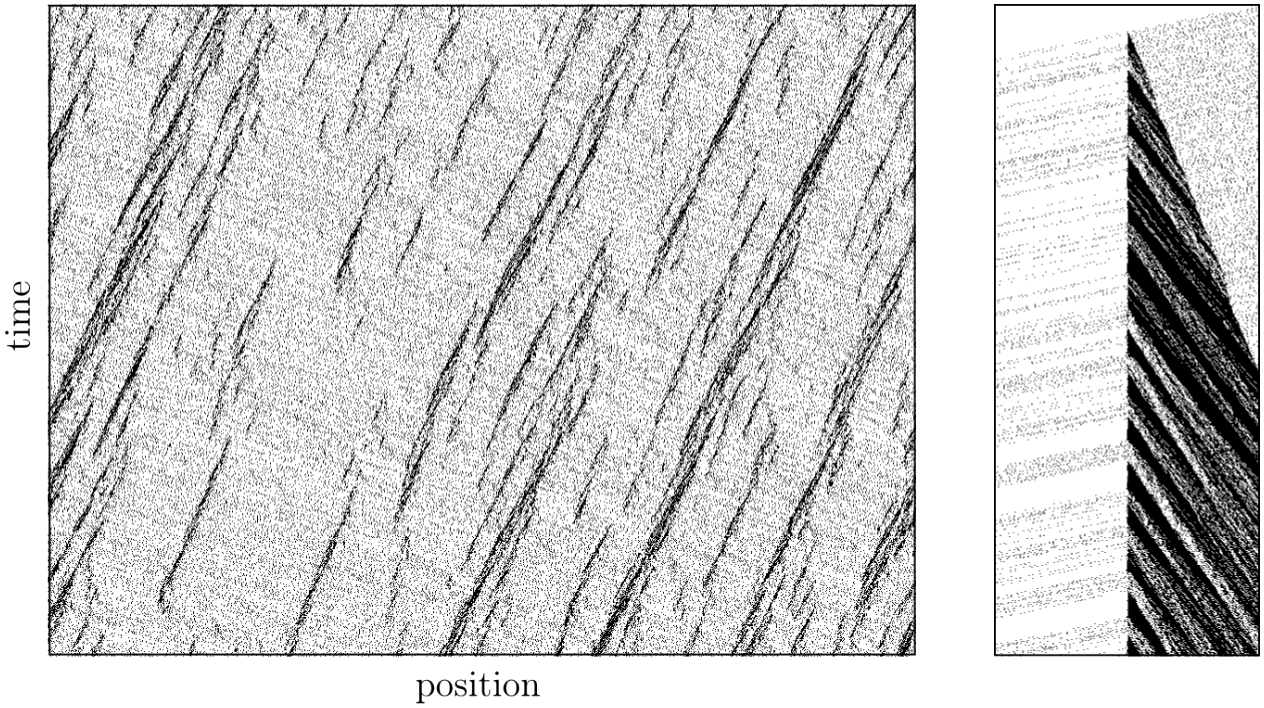

Figure 4.2: Translation dependence

4.3 Intersection Mean-Field Approximation

The extension of the above solution method to the proposed intersection model inserts the additional stopping rules relevant to the intersection in the braking stage. Under the mean-field assumption, the probability of an intersection-specific stopping rule $p(rule)$ being in effect for a particular vehicle can be broken down into:

- $p(location)$: the probability of the vehicle being located in a position for the rule to apply
- $p(turn)$: the probability of a vehicle's turn decision being subject to the given rule
- $p(light)$: the probability of the given rule being in effect based on the light state
- $p(occupation)$: the probability of other vehicles occupying positions which trigger the rule

$$p(rule) = p(location)p(turn)p(light)p(occupation) \tag{4.8}$$

Each of the intersection stopping rules can be cast into the form above.

4.3.1 Deviation from mean-field approximation

The approximation that both density and average velocity are equal everywhere violates conservation equations at the cells inside the intersection. If two approach lanes have average velocity v and density ρ, the resulting flow is $J = \rho v$ from each approach and the total inflow is $2\rho v$. The velocity mean-field approximation is assumed within the intersection and the density at the intersection is calculated as the sum of the inflowing densities (that is, assuming intersection-cell vehicle density $\rho_i = 2\rho$ and velocity $v_i = v$ instead of $\rho_i = \rho$ and $v_i = 2v$). The inflow per cell inside the intersection can be calculated by summing all incoming streams: $3L + 2T + R$, as show in Figure 4.3 This value appears as the denominator

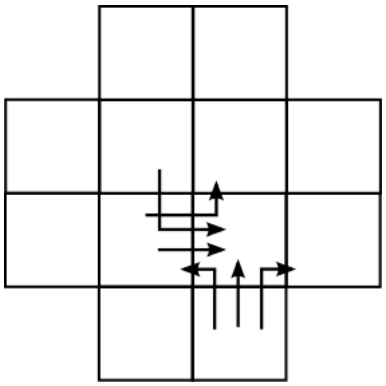

Figure 4.3: Trajectories passing through intersection cell

in the expressions for the probability of several rule's application. In contrast, without the above reasoning, the same denominator would appear as $L + R + T = 1$.

The following symbols help to reduce the number of expressions in the mean-field calculation.

$$\begin{aligned} C_I &= 3L + 2T + R \\ f_p &= T + L \\ f_g &= \frac{4L + 2T}{C_I} \end{aligned} \tag{4.9}$$

4.3.2 Rule (1): High priority

Rule (1) provides the criteria for admitting right and left turns into higher-priority traffic streams. It is in effect for left-turning traffic when crossing the stream of on-coming traffic (during a green light) and for right-turning traffic entering the intersection during a red light. This rule also applies when a straight-through or left-turning vehicle is caught in the intersection after the light turns red although such cases should be rare. Figure 4.4 illustrates cells subject to these rules for northbound traffic only.

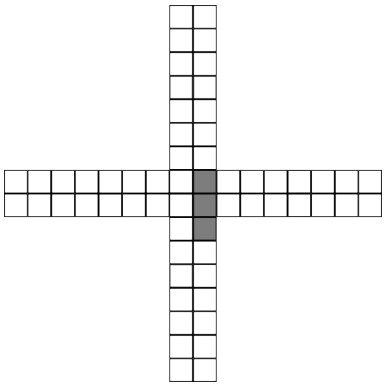

Figure 4.4: Priority Yielding Effect Area

The cells for which this rule is in effect can be treated separately to illustrate how the rule applies in each situation.

The priority rule is in effect at the uppermost cell (left figure in Figure 4.5) when left-turning traffic is yielding to left-turning or straight-through traffic during a green light. In this

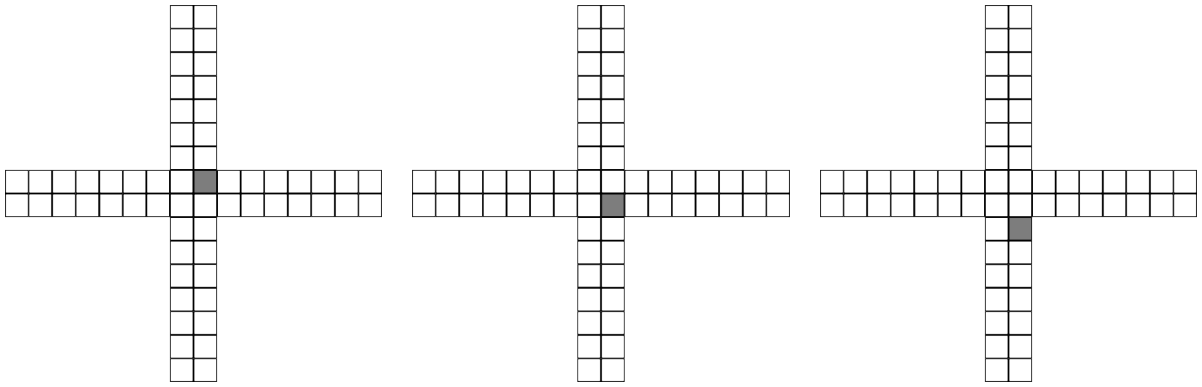

Figure 4.5: Individual Priority Yielding Cells

situation:

$$\begin{aligned} p(location) &= \frac{1}{4+2a} \\ p(turn) &= L \\ p(light) &= s \\ p(occupation) &= c_1 f_p \end{aligned} \tag{4.10}$$

When right-turning traffic yields to straight-through or left-turning traffic during a red light (right figure in Figure 4.5):

$$\begin{aligned} p(location) &= \frac{1}{4+2a} \\ p(turn) &= R \\ p(light) &= 1-s \\ p(occupation) &= \frac{2c_1 f_p}{C_I} \end{aligned} \tag{4.11}$$

Owing to the probabilistic braking rule, a situation can occur where a straight-through or left-turning vehicle stops inside the intersection until the light changes color (turns red). This vehicle must now yield to straight-through traffic with the right of way. The middle image of Figure 4.5 illustrates the cell where a vehicle would stop under this rule.

$$\begin{aligned} p(location) &= \frac{1}{4+2a} \\ p(turn) &= L+T \\ p(light) &= 1-s \\ p(occupation) &= c_1 f_p \end{aligned} \tag{4.12}$$

4.3.3 Rule (2): Red light

Rule (2) causes all vehicles to stop upon arrival at the intersection during a red light; this is only necessary for right-turning traffic during a red light. Left and right turning traffic stop too; however, they are also dealt with by rule (3) whereas this rule allows right-turning traffic to continue after stopping initially. Figure 4.6 illustrates the area subject to this rule for northbound traffic.

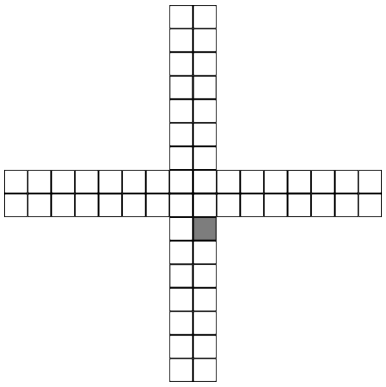

Figure 4.6: Stop Upon Arrival Effect Area

When $v_{max} = 1$, the probability of rule (2) affecting a vehicle is 0; this rule is only noticeable for vehicles with $v_{max} > 1$ since vehicles accelerate by 1 unit per timestep if below v_{max}. The vehicle's acceleration at the start of the next timestep means that when the vehicle's movement is calculated at the end of the next timestep, it is in the same state whether it had been subject to rule (2) or not.

4.3.4 Rule (3): Red light, right turning

Rule (3) prevents left-turning and straight-through traffic from entering the intersection during a red light, while allowing right-turning traffic to proceed. Figure 4.7 illustrates the area subject to this rule for northbound, left-turning or straight-through traffic.

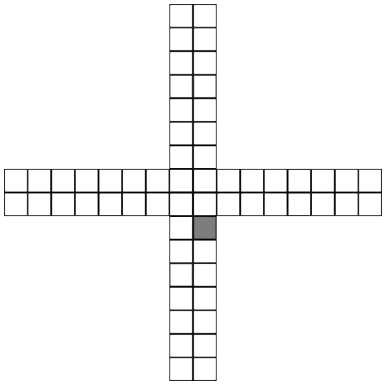

Figure 4.7: Waiting at Red Effect Area

For rule (3):

$$\begin{aligned} p(location) &= \frac{1}{4+2a} \\ p(turn) &= L+T \\ p(light) &= 1-s \\ p(occupation) &= 1 \end{aligned} \tag{4.13}$$

4.3.5 Rule (4): Turning

Rule (4) causes turning traffic to stop travelling down the original (approach) road upon arrival at the destination lane. This rule applies in different locations for left and right-turning vehicles. The image on the left-hand side of Figure 4.8 illustrates the area subject to rule (4) for northbound, left-turning traffic and the image on the right illustrates the area subject to rule (4) for northbound, right-turning traffic.

Like rule (2), this rule does not affect vehicles with $v_{max} = 1$. Each vehicle can reduce

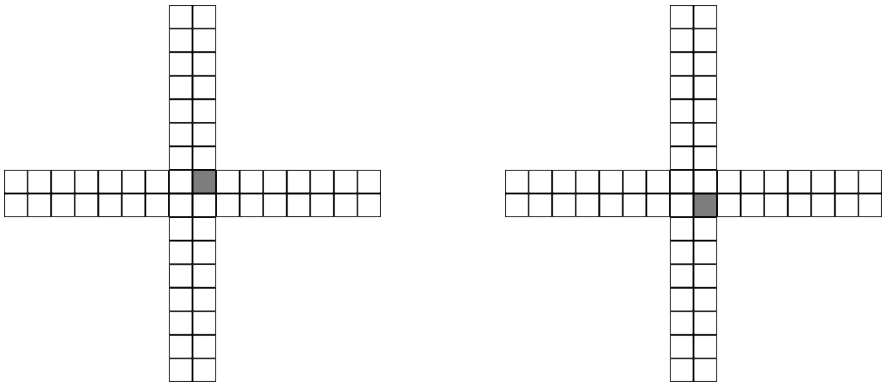

Figure 4.8: Left and right turn stop effect areas

its speed upon arriving at the turn lane by 1 unit at most which will be regained in the acceleration phase at the start of the next timestep.

4.3.6 Rule (5): Late occupation

Rule (5) prevents right-turning vehicles from entering an intersection if the cell in the near-left corner of the intersection is occupied by a left-turning or nonturning vehicle heading toward the right-turning vehicle. Out of the six possible trajectories which a vehicle in a given cell may have, three could conflict with traffic if the light changes. This yields occupation probability cf_g. Figure 4.9 illustrates the area subject to this rule for right-turning traffic during a green or red light.

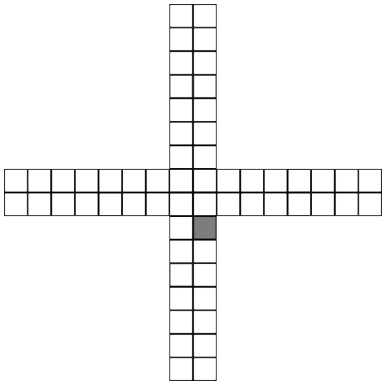

Figure 4.9: Intersection Occupied Stop Effect Area

For rule (5):

$$\begin{aligned} p(location) &= \frac{1}{4+2a} \\ p(turn) &= R \\ p(light) &= 1 \\ p(occupation) &= cf_g \end{aligned} \tag{4.14}$$

4.3.7 Rule (6): Gridlock

Rule (6) prevents left-turning and straight-through traffic from entering an intersection if the cell on the opposite side of the intersection is occupied by a left-turning or straight-through vehicle from a previous green light or a left-turning vehicle travelling in the same direction. This prevents gridlock from occuring, a situation which can never resolve in this model. As in rule (5), the possibility that a vehicle can stop for an unlimited amount of time means that vehicles can remain in the intersection from previous lights. Out of the six possible trajectories which a vehicle in a given cell may have, three could conflict with traffic if the light changes. This yields occupation probability cf_g. Figure 4.10 illustrates the area subject to this rule for northbound, left-turning and straight-through traffic during a green light.

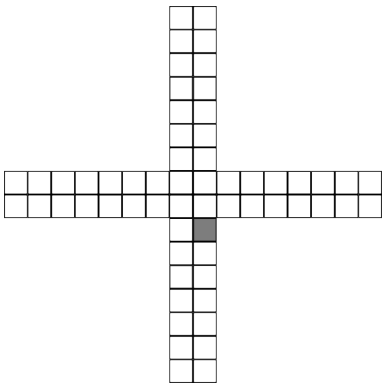

Figure 4.10: Gridlock Stop Effect Area

For rule (6):

$$\begin{aligned} p(location) &= \frac{1}{4+2a} \\ p(turn) &= L+T \\ p(light) &= s \\ p(occupation) &= cf_g \end{aligned} \tag{4.15}$$

4.3.8 Combining the rules

The probability of braking due to intersection-specific rules can be calculated for each cell individually. The probability of braking in a given cell is equal to the probability of at least one of the rules being active for that cell. For a given lane of traffic in the intersection (take northbound for example), there are only three cells at which the intersection rules apply. Rule (1) is an example of a rule which may apply at any of the three possible intersection cells on the northbound lane as in Figure 4.4. Starting with the bottom cell (just ouside the intersection), the rules which may be in application are (1), (2), (3), (5) and (6). Rule (1) at this location only applies to right-turning traffic during a red light. Rule (2) is not included in Figure 4.11 since traffic with $v_{max} = 1$ is not affected. Rule (3) only affects left-turning and straight-through traffic during a red light. Rule (5) only affects left-turning traffic during a green light and right-turning traffic during a red light. Rule (6) affects left-turning and straight-through traffic during a green light. For the following derivation, $v_{max} = 1$.

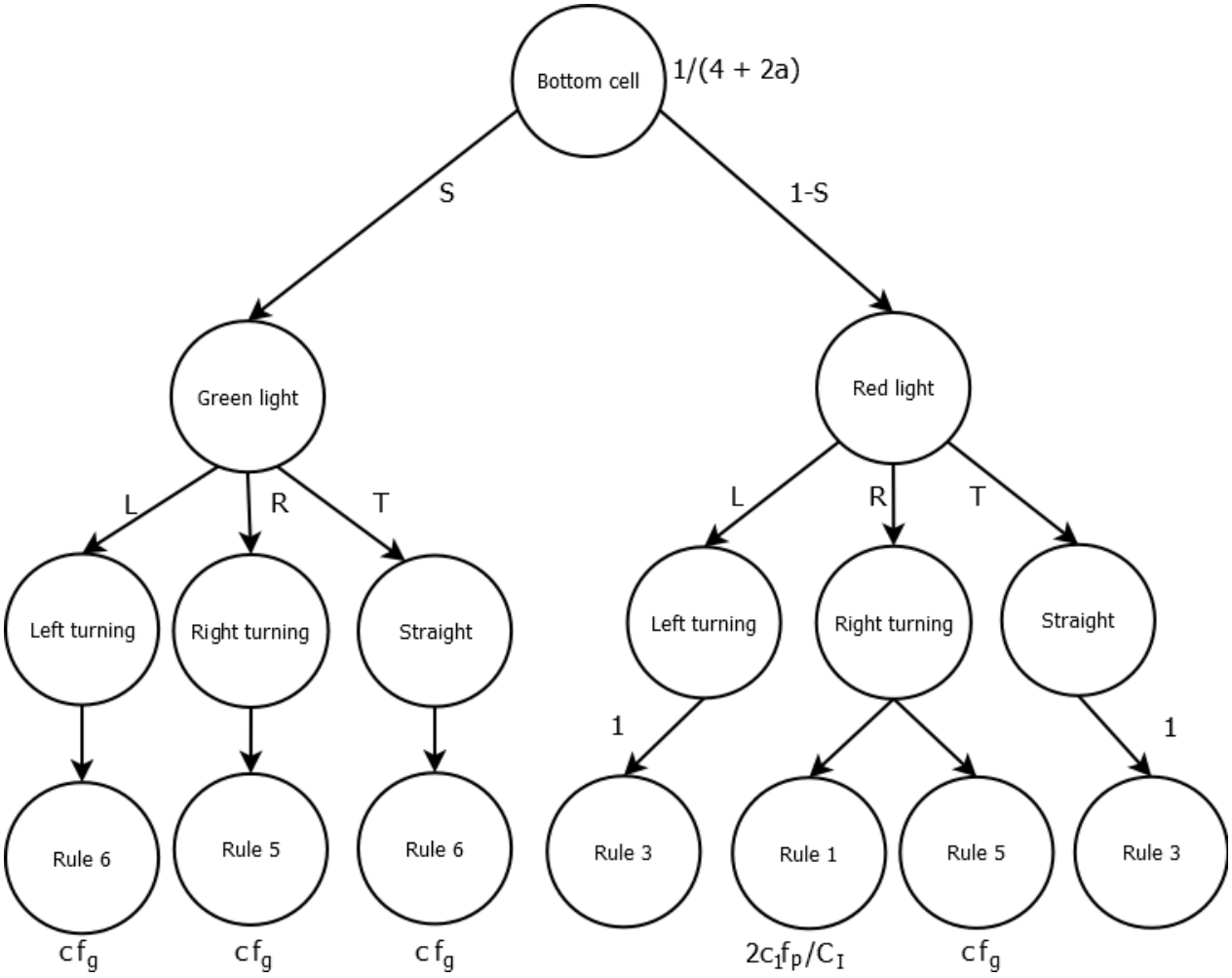

Figure 4.11: Bottom cell stop-rule probability tree

In the middle cell, the rules which may be in application are (1) and (4). Rule (1) causes traffic stopped in the intersection to yield to incoming straight-through traffic. Rule (4) prevents right-turning traffic from travelling beyond the destination lane. Rule (4) is does not affect traffic when $v_{max} = 1$ and is not included in Figure 4.12.

In the top cell, the rules which may be in application are (1) and (4). Rule (1) causes left-turning traffic to yield to oncoming straight-through traffic during a green light. Rule (4) prevents left-turning traffic from travelling beyond the destination lane. Again, Rule (4) does not affect traffic when $v_{max} = 1$ and is not included in Figure 4.12.

Summing probabilities of the branches resulting in application of braking rules yields the

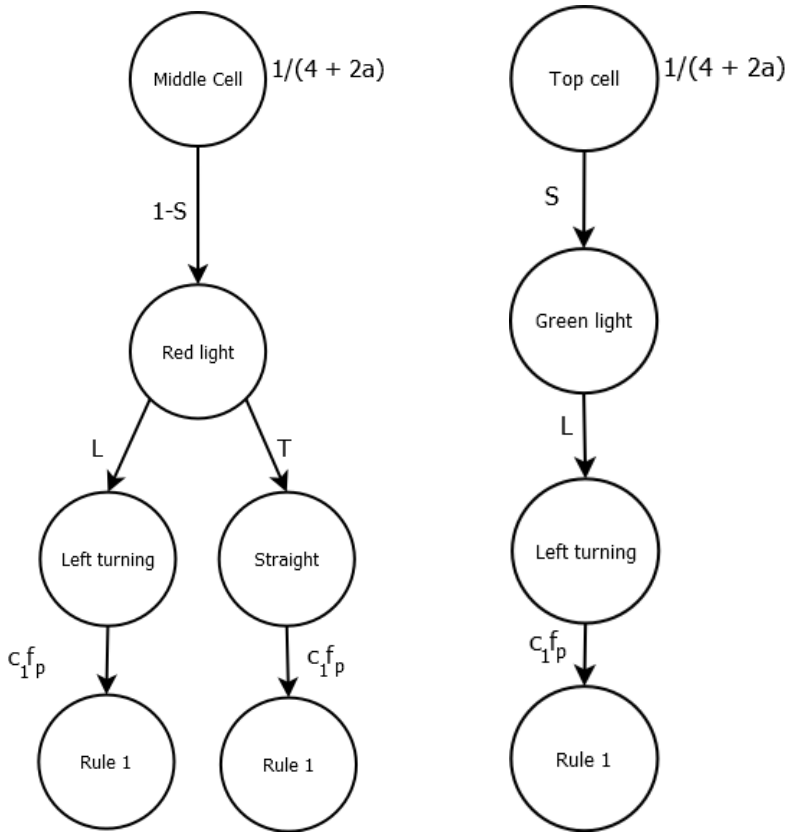

Figure 4.12: Middle cell (left) and top cell (right) stop-rule probability trees

total probability P_I of an intersection-related braking rule being in application.

$$P_I = \frac{s((T+L)cf_g + Lc_1f_p) + (1-s)(L + T + R(cf_g + \frac{2c_1f_p}{C_I}) + c_1f_p^2)}{4 + 2a} \tag{4.16}$$

This expression can be simplified and rearranged: rule (1) in the middle cell (the $c_1f_p^2$ term) is dropped because the mean-field approximation is likely to overestimate it. Rule (1) only occurs in the middle cell if cars are stuck in the intersection after the light changes, i.e. at the light transition. The occurance of rule (1) should therefore be related to the frequency of light switching, with a longer light period corresponding to a lower rate of occurances of rule (1) in the middle cell. For a period of 30 timesteps (equivalent to approximately 30 seconds of real time), an intersection would undergo one switching timestep. The relative rarity of the switching timesteps compared to nonswitching timesteps is the reason for the overestimation of the rate of rule (1) occurance in the middle cell by the mean-field approximation. P_I

becomes

$$P_I = \frac{sf_p(cf_G + Lc_1) + (1-s)(f_p + R\frac{2c_1 f_p}{C_I}) + Rcf_g}{4 + 2a} \tag{4.17}$$

This expression is somewhat easier to interpret. The terms multiplied by s are those whose probability increases with the proportion of green light. The terms multiplied by $(1-s)$ are those whose probability increases with the proportion of red light. The numerator terms not multiplied by s or $(s-1)$ are those whose probability is not related to the proportion of red or green light. Inside the s term, the expression $f_p L c_1$ is due to left-turning traffic yielding to oncoming traffic. The expression $f_p c f_g$ is due to left and straight-through traffic avoiding gridlock. Inside the $(1-s)$ term, f_p is due to left and straight-through traffic stopping at red lights. The expression $R\frac{2c_1 f_p}{C_I}$ derives from right-turning traffic yielding to higher priority traffic during a red light. The Rcf_g term outside s or $(s-1)$ in the numerator is due to right-turning traffic stopping because of the "intersection occupied" rule (rule 5).

$$\begin{aligned} P_{I,avg} &= \frac{(s_{NS} + s_{EW})(f_p(cf_g + Lc_1)) + (2 - s_{NS} - s_{EW})(f_p + R\frac{2c_1 f_p}{C_I}) + 2Rcf_g}{4 + 2a} \\ P_{I,avg} &= \frac{f_p(cf_g + Lc_1) + f_p + R\frac{2c_1 f_p}{C_I} + 2Rcf_g}{4 + 2a} \end{aligned} \tag{4.18}$$

A symmetric light timing of $s_{NS} = s_{EW} = 0.5$ is assumed. The above expression for P_I can be integrated into the original solution for the NaSch model as follows. The initial update rule (acceleration) is applied as in the standard NaSch model.

$$\begin{aligned} c_0(i, k + 1/4) &= 0 \\ c_1(i, k + 1/4) &= c_0(i, k) \end{aligned} \tag{4.19}$$

In Figure 4.3, traffic brakes according to the standard braking rule. Here the proportion of

traffic braking due to the intersection-specific rules can also be inserted. Figure 4.3 becomes

$$\begin{aligned} c_0(i, k + 2/4) &= c_0(i, k + 1/4) + (c(i + 1, k + 1/4) + P_I)c_1(i, k + 1/4) \\ c_1(i, k + 2/4) &= c_1(i, k + 1/4)(d(i + 1, k + 1/4) - P_I) \end{aligned} \tag{4.20}$$

The randomization rule is applied in the same manner:

$$\begin{aligned} c_0(i, k + 3/4) &= c_0(i, k + 2/4) + pc_1(i, k + 2/4) \\ c_1(i, k + 3/4) &= qc_1(i, k + 2/4) \end{aligned} \tag{4.21}$$

The movement update is also applied in the same manner:

$$\begin{aligned} c_0(i, k + 1) &= c_0(i, k + 3/4) \\ c_1(i, k + 1) &= c_1(i - 1, k + 3/4) \end{aligned} \tag{4.22}$$

Removing dependence on time and position:

$$\begin{aligned} c_0 &= c(c + pd + qP_I) \\ c_1 &= qc(d - P_I) \end{aligned} \tag{4.23}$$

Together, equations 4.17 and 4.23 give a rough description of the relationship between intersection parameters and flow rates for the case $v_{max} = 1$. As would be expected, a higher P_I yields lower flow. The limit $\lim_{a\to+\infty} P_I$ approaches zero; as the approach lengths grow longer, the dynamics approach that of a single NaSch road. Equation 4.23 is not an expression of c_1 in terms of other variables—c_1 is a parameter of P_I. Solving for c_1 independently, split P_I into a linear function of c_1:

$$\begin{aligned} P_{I,avg} &= A + Bc_1 \\ A &= \frac{cf_pf_g + f_p + 2Rcf_g}{4 + 2a} \\ B &= \frac{f_pL + 2R\frac{f_p}{C_I}}{4 + 2a} \end{aligned} \tag{4.24}$$

Now c_1 can be written in terms of A and B:

$$c_1 = \frac{(qc)(d - A)}{1 + qcB} \tag{4.25}$$

Chapter 5

Data Collection

A video-based vehicle tracking system was designed in order to verify the predictions of this model. Individual turns must be detected in order to measure the macroscopic turn proportions (L, R, T). The number and velocity of vehicles must be measured to estimate density c (linear with vehicle count since the area under observation is constant) and average velocity v_{avg}.

This is accomplished using preprocessing to isolate the moving parts of the image followed by Multiple Hypothesis Tracking (MHT) [Reid 1979], a data-association algorithm used in assigning object detections to multiple targets (vehicles). MHT (and underlying Kalman filters) provides an estimate of a vehicle's velocity and position in the image plane (pixel coordinates). Turns are detected based on the location of initial and final positions.

5.1 Video Recordings

Videos were recorded at Robart's Library, University of Toronto (130 St. George St., Toronto, ON, Figure 5.1) at the intersections of Huron and Harbord street, St. George and Harbord street and Huron and Sussex street. These are all signalised intersections with four approaches as in the model; however, they have left-handed turning lanes which reduce the negative impact of left-turning vehicles.

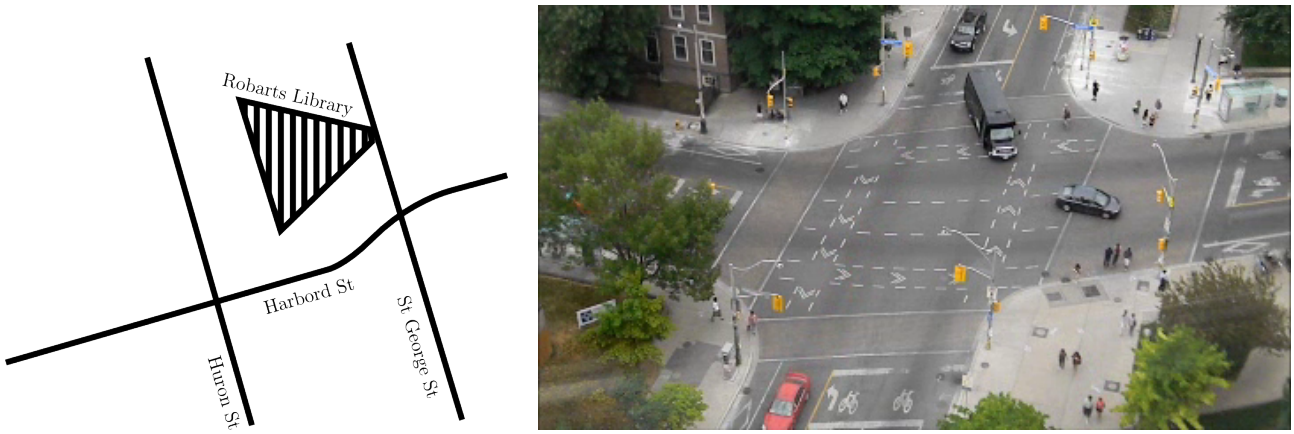

Figure 5.1: Video footage location

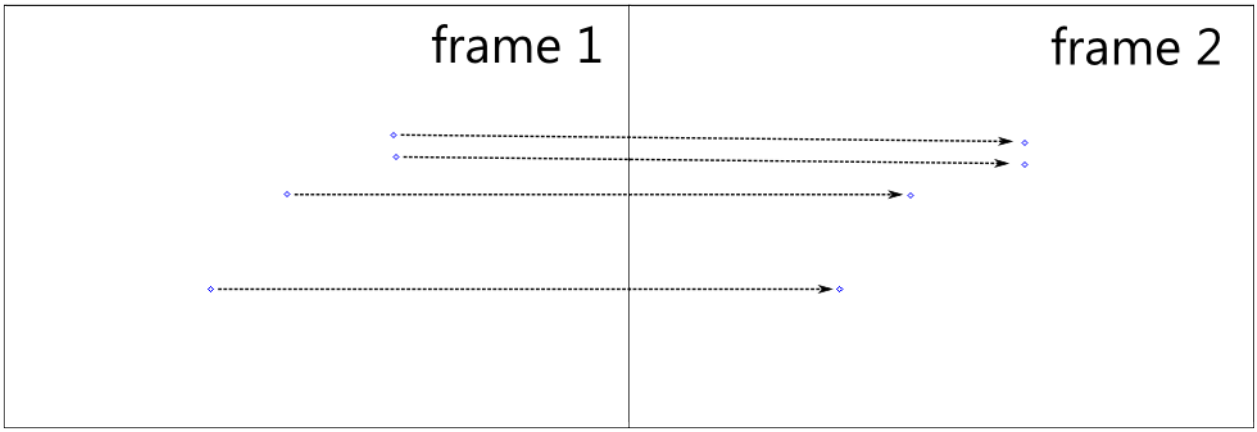

Figure 5.2: Measurement association

5.2 Multiple Object Tracking

The problem of tracking multiple objects can be separated into two subproblems. First, objects are detected. This yields an estimate of object locations. However, it does not yield an estimate of speed and is susceptible to false positives. Furthermore, simply detecting objects independently in each frame does not allow for turn detection. A method for associating detections with individual vehicles is necessary. In Figure 5.2, any of the four measurements in the left-hand figure could be a new vehicle or false positive. Each of the measurements in the right-hand figure could be a new vehicle, a false measurement or another measurement from a vehicle existing in the first frame. Even considering only two frames, a significant

Figure 5.3: Position and velocity estimates

number of measurement association permutations must be considered. Multiple Hypothesis Tracking provides a position and velocity estimate for a variable number of vehicles using a rolling window to defer measurement assignments until more frames are recieved. The green circles indicate position covariance in Figure 5.3 and the red lines indicate velocity estimates.

5.2.1 Background Subtraction

The first step in performing object detection is background subtraction. For this, an estimate of the background is necessary (Figure 5.4). This is done by averaging all frames in a video (processing is done offline although a rolling background calculation might be possible for real-time applications). The background estimate is then subtracted from each video frame.

5.2.2 Blob fitting

At the first stage, object detection is perfomed independently on a frame by frame basis. The two-dimensional cross correlation is calculated between the thresholded movement image

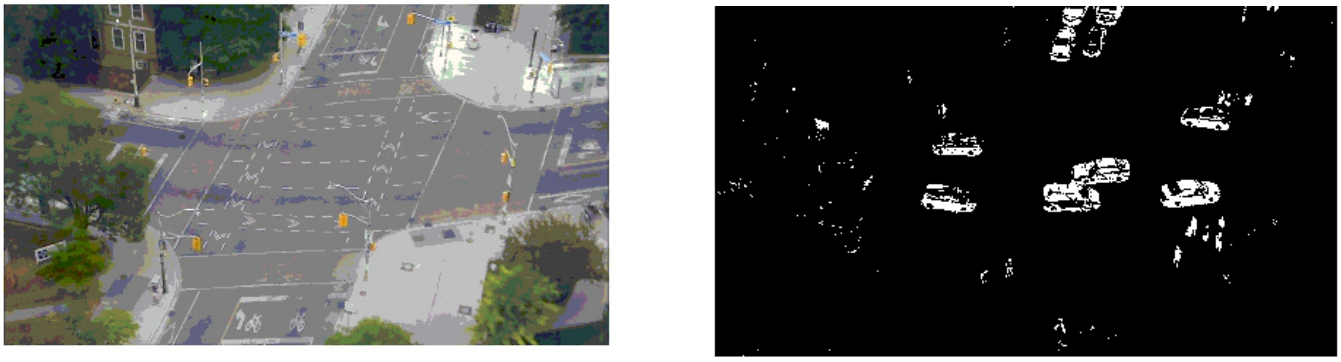

Figure 5.4: Background frames (left) and movement frames (right)

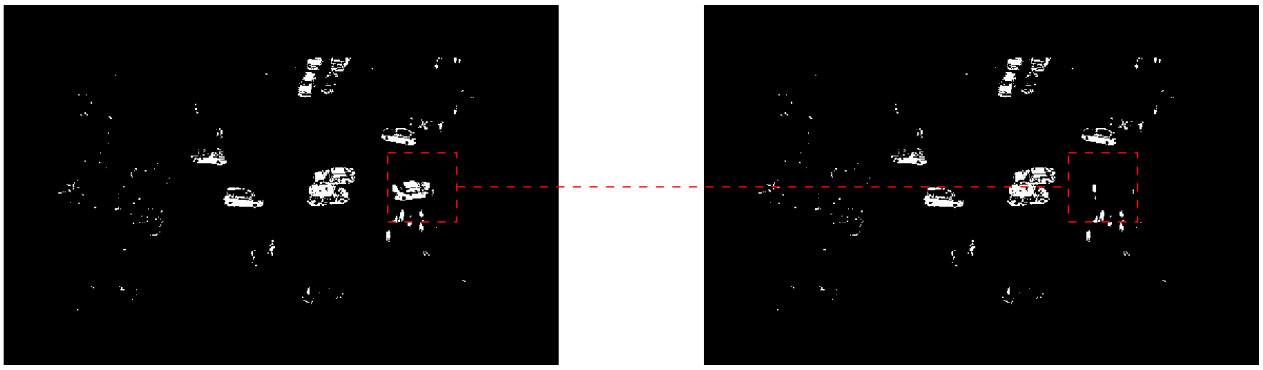

Figure 5.5: Blob deletion

and a circular prototype of a fixed radius (selected by hand for each video to be processed). This operation smooths out fine details in individual vehicles and removes high-frequency noise in the image. The peak value in the cross correlation is taken to be the most likely positon to find a vehicle. The radius surrounding this point is cleared in the thresholded movement image (Figure 5.5), thereby accounting for the vehicle. This operation is repeated for however many vehicles are expected in an image. The number of expected vehicles is approximated as a linear function of the number of white pixels in the movement frame. The entire image's cross correlation is not recomputed; only the area affected by the last cleared region. Figure 5.6 illustrates the change in the cross-correlation image after erasing a single vehicle from the movement mask. The affected region is limited to the area around the deleted vehicle. Recalculating only this region can reduce blob-fitting computation time

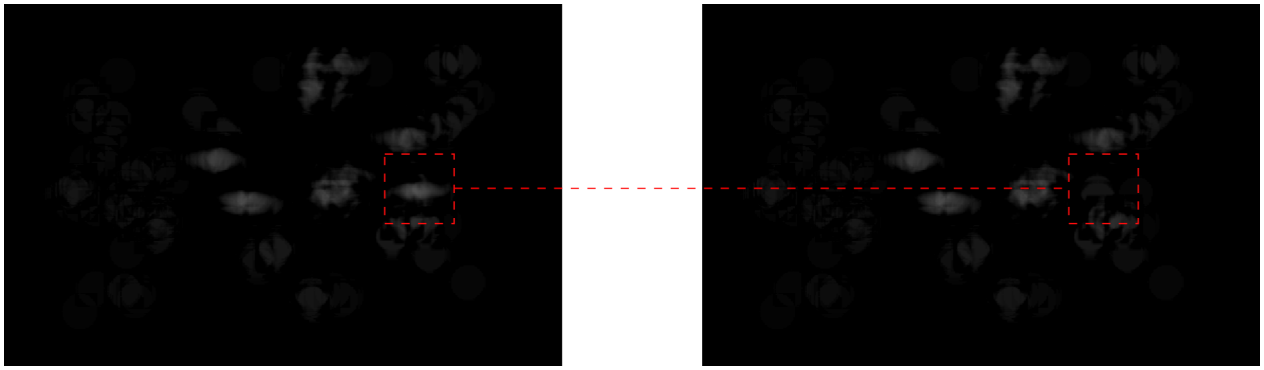

Figure 5.6: Cross correlation after deletion

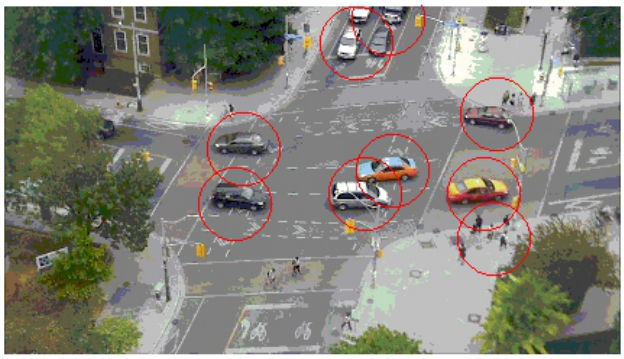

Figure 5.7: Object detections

by 5-10 times. Each peak location is recorded as the location of a vehicle. The results of this operation are show in Figure 5.7. The code used to perform blob fitting has been released to the public on the Mathworks file exchange at the following URL:

`http://www.mathworks.com/matlabcentral/fileexchange/33953-blob-fitting`

5.2.3 Multiple Hypothesis Tracking

MHT is a popular technique for associating object measurements with tracked objects originally described by Reid [1979]. Blackman [2004] discusses common implementation variations. In its simplest form, MHT considers all possible associations between object detections and tracked objects. The initialization frame is treated at the root node of a hypothesis tree. Each node contains a single possible interpretation of measurement-object assignments. As

each successive frame arrives, each node is expanded into all possible interpretations of the new data. The state is estimated by selecting the object-measurement assignment sequence yielding with the highest probability according to individual object dynamics and object measurement statistics. The original algorithm's computation requirements are exponential in object number and time and is therefore not realistic for implementation. The measurement assignment tree can be pruned heavily to achieve a serial (near real-time) object tracking algorithm as described by Cox & Hingorani [1996]. This is achieved through an implementation of Murty's algorithm [Murty 1968] which provides a list of the k-best measurement assignment hypotheses. More complex pruning methods described by Cox & Hingorani [1996] (splitting and merging) are not used in the MHT implementation used for this study.

5.3 Object Movement Model for Multiple Hypothesis Tracking

MHT requires an underlying Kalman filter motion and observation model for individual vehicles in order to evaluate branch probabilities. A standard two-dimensional translation model is used. Position x, y and velocity v_x, v_y are represented in image coordinates (pixels). The motion matrix $\mathbf{A}$ corresponds to translational motion. Observation matrix $\mathbf{H}$ only allows direct observation of position.

$$\dot{\mathbf{x}} = \mathbf{A}\mathbf{x} \qquad \mathbf{x} = \begin{bmatrix} x \\ v_x \\ y \\ v_y \end{bmatrix} \qquad \mathbf{y} = \mathbf{H}\mathbf{x} \tag{5.1}$$

$$\mathbf{A} = \begin{bmatrix} 1 & dt & 0 & 0 \\ 0 & 1 & 0 & 0 \\ 0 & 0 & 1 & dt \\ 0 & 0 & 0 & 1 \end{bmatrix} \qquad \mathbf{H} = \begin{bmatrix} 1 & 0 & 0 & 0 \\ 0 & 0 & 1 & 0 \end{bmatrix} \tag{5.2}$$

$$\mathbf{Q} = \begin{bmatrix} \frac{(dt)^3}{3} & \frac{(dt)^2}{2} & 0 & 0 \\ \frac{(dt)^2}{2} & dt & 0 & 0 \\ 0 & 0 & \frac{(dt)^3}{3} & \frac{(dt)^2}{2} \\ 0 & 0 & \frac{(dt)^2}{2} & dt \end{bmatrix} \qquad \mathbf{R} = \begin{bmatrix} 35 & 0 \\ 0 & 35 \end{bmatrix} \tag{5.3}$$

All measurements are pixel coordinates in the image plane. A standard Kalman filter is used in calculating measurement assignment probabilities; $\mathbf{Q}$ and $\mathbf{R}$ are the process and observation covariance matrices. These motion models are taken from Cox & Hingorani's [1996] two-dimensional movement tracking implementation. The measurement noise variance $\mathbf{R}$ was tuned by hand.

5.4 Murty's *K*-Best Assignment Algorithm: Rectangular Implementation

Some method of generating the k-best measurement associations is necessary for a practical MHT implementation as described in Cox & Hingorani [1996]. Murty's [1968] algorithm provides measurement associations (instances of the linear assignment problem) in order of the optimal association followed by the $k-1$ next-best associations. An existing script by Eric Trautmann available through MATLAB MathWorks implemented Murty's algorithm for square matrices. This applies when the number of measurements is equal to the number

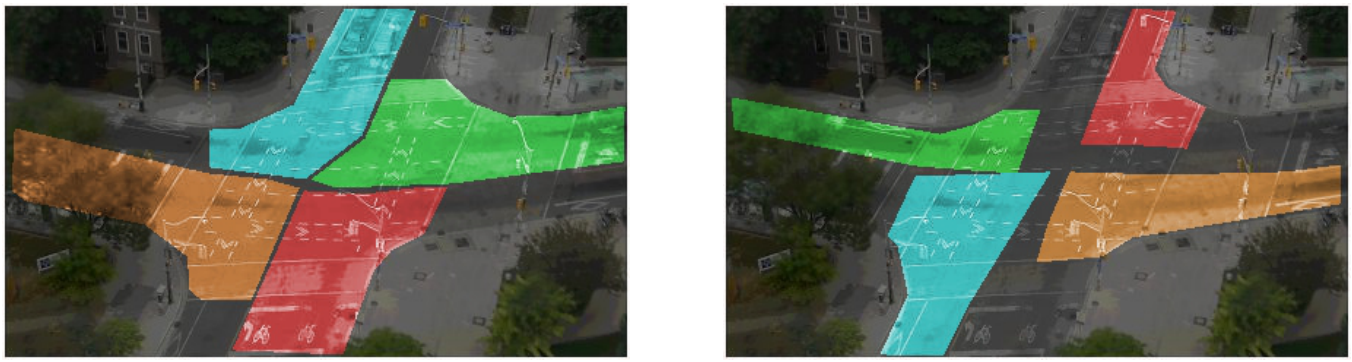

Figure 5.8: Approach and exit region polygons

of targets being tracked. In this application, the number of measurements may be more or less than the number of vehicles in each frame due to false positives, multiple measurements of a single vehicles or misses. The existing code was adapted by the author to treat the case of rectangular assignments as well as square. Note that this implementation does not allow assignment of multiple measurements to a single vehicle; it only allows consideration of measurement sets which are not equal in size to the target set. In principle, it is possible to assign multiple measurements to a vehicle using MHT. In this application, the chances of detecting multiple measurements from a single vehicle is mostly a function of perspective distortion; vehicles closer to the camera appear larger. This effect is minimised by using a long focal length and recording footage from a high perspective. Further correction could be performed using a perspective transformation calculated using the geometry of the camera placement relative to the intersection.

5.4.1 Turn detection

5.4.1.1 Turn detection with initial and final position

Polygons covering the approaches and exits (Figure 5.8) are manually selected. By tracking the polygon a vehicle occupies at the time of detection and deletion, the vehicle's turn decision can be detected. For objects originating or exiting outside of any polygon, the trajectory is considered unknown. Figure 5.9 illustrates the results of polgyon-based turn detection. By

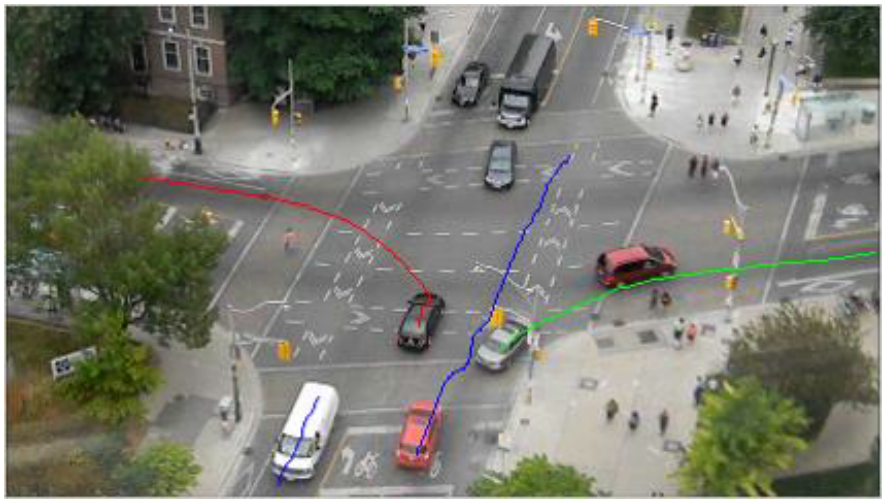

Figure 5.9: Instantaneous Turn Proportion Measurement: Red (left), Green (right), Blue (straight)

storing the results of object tracking, each object's initial and final positions may be known at each frame. This allows an instantaneous estimate of which way each vehicle is turning; this in turn allows an instantaneous estimate of turn proportion variables L, R, T.

5.4.1.2 Turn measurement causality

One problem with trying to measure the effect of turn proportion on flow rate is that turn detection is easiest after the turn has occured. Therefore, any measurement of the current turn proportion using a delayed detection gives an outdated estimate. This problem is addressed by recording the full trajectory of each vehicle and saving it for postprocessing. This allows the turn decisions of all vehicles to be known upon detection.

5.5 Code Architecture

The software for tracking vehicles and counting turns was written in a combination of C# and MATLAB languages (Figure 5.10). The MHT algorithm requires a tree structure and as MATLAB has no native tree structure, some alternative is needed. The two components communicate through MATLAB's .NET object support. The code is a combination of existing

(open source) and newly written code.

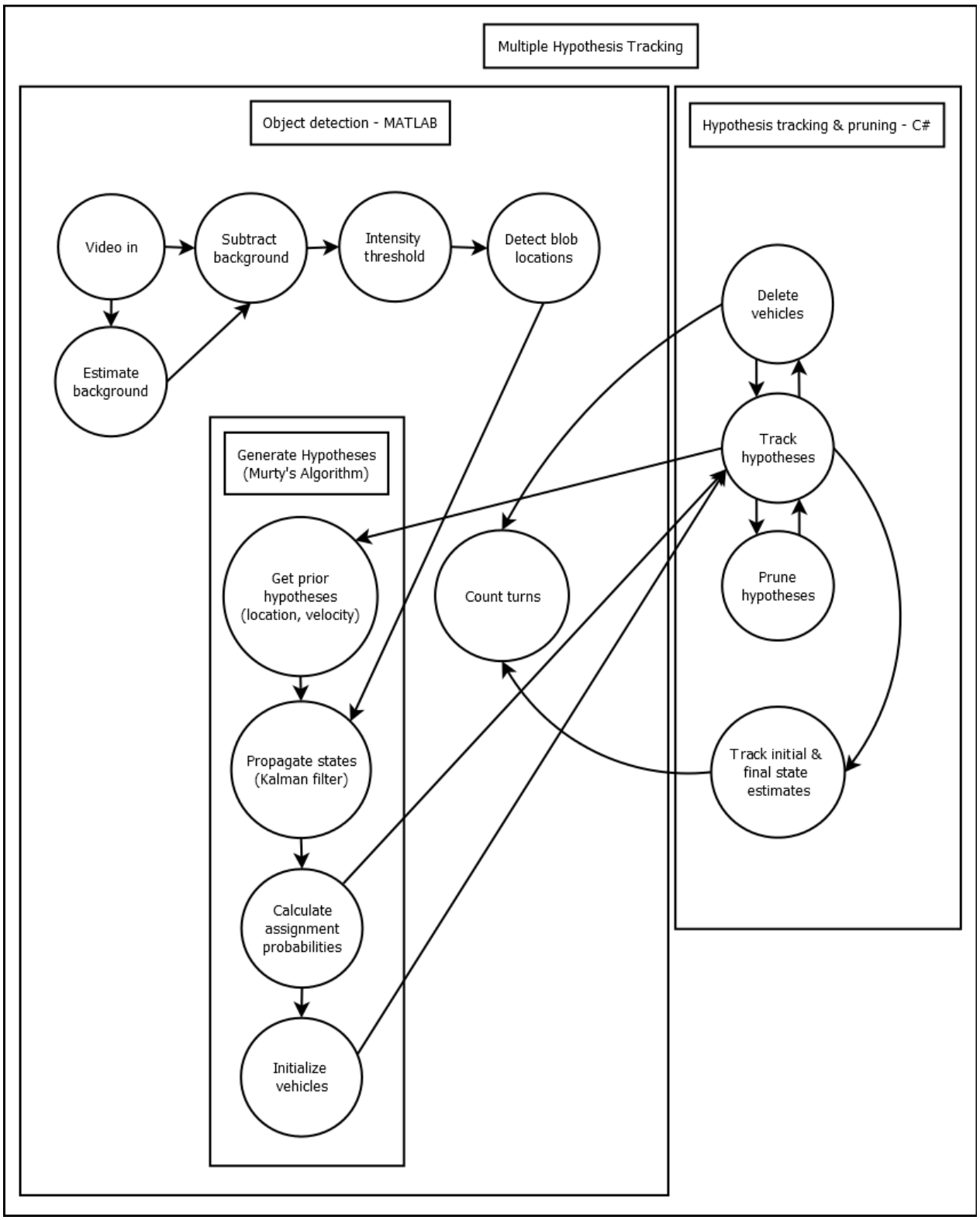

Figure 5.10: MHT Implementation Architecture

5.6 Sources of error

5.6.1 Vehicle definition

To track individual vehicles, some notion of what constitutes an individual vehicle is necessary. Summed intensity of the movement frame might seem naive; it often results in multiple detections of large vehicles. However, multiple detection of large vehicles can provide more information about the effective amount of traffic in an intersection. A single detection of each vehicle plus a size estimate would ideally provide the most accurate description of the situation but failing this, multiple detections might be preferrable to single indistinguishable detections.

5.6.2 Pedestrians

Pedestrian traffic appears to affect left- and right-turning traffic significantly. Pedestrians are not represented at all in the intersection model although there is nothing preventing this. The object tracking algorithm attempts to identify pedestrians by position of origin and can eliminate them from vehicle counts. Pedestrians are not counted or tracked accurately; the object tracking filters are tuned for vehicle movement and size. This results in individual pedestrians being ignored and large groups being detected. It can be difficult to filter out all pedestrian detections based on location (outside the road area of the intersection) since pedestrian groups tend to coalesce at crosswalks, right on the edge of the intersection area. One possible way to eliminate this would be to perform some visual *a posteriori* classification of detected objects. Detections classifed as originating from vehicles and pedestrians could be tracked by parallel MHT algorithms with individual filter parameters.

5.6.3 Object interference

The prototype cross correlation function can yield a peak between two nearby vehicles instead of two separate peaks for each vehicle. The prototype can be shrunk but this has the tradeoff

of detecting smaller, unwanted objects more often.

5.6.4 Poor background model

Errors in calculation of the background model come from several sources. First, the exposure autocorrections described above mean that different parts of the video are taken at different exposure values. Second, stationary vehicles in the frame can cause a negative image when they leave and thus false positives. Also, when calculating the background for a long video, roundoff error becomes an issue. If a small enough fraction of each frame is added to the background estimate, division error becomes significant. Downsampling the video for background calculation is one way of mitigating this problem.

5.6.5 Road-colored cars

Grey and black vehicles tend to be detected poorly since subtraction of the background yields a low difference. Again, eliminating problems due to exposure correction and by extension a poor background model could allow a lower threshold in the movement mask calculation. This would provide a better chance of detection cars similar in color to the road.

5.7 Performance

Figure 5.1 provides a manual measurement of the vehicle count error at 30 second intervals from a sample video. The larger errors are due to frames with small vehicles at the far corner of the intersection and larger vehicles closer to the camera.

Table 5.1: Vehicle Count Error Measurements

Time (mm:ss)	Error (fraction)	Error (%)
00:00	0/4	0
00:30	1/2	50
01:00	3/9	33
01:30	1/6	17
02:00	0/2	0
02:30	0/2	0
03:00	6/10	60
03:30	3/8	37
04:00	3/10	30
04:30	7/13	54
05:00	3/9	33
05:30	2/7	29

Table 5.2: Turn Count Error Measurements

Turn	Total	Counted	Error (absolute)	Error (%)
Left	7	4	3	43
Right	9	20	11	120
Straight	81	62	19	23

Chapter 6

Measurements Compared to Model Predictions

6.1 Flow-vs-turn proportion

The results of the mean-field approximation, simulation and video measurement are compared below. The data used in this section is taken from the intersection at Harbord St. and St. George St. in Toronto over a two-hour period. The turn counting software reports 17 left turns, 66 right turns, 128 nonturning vehicles, 2387 trajectory paths discarded for being too short (under 30 pixels or about 3 car lengths), 181 discarded for not originating and exiting in a known approach-exit polygon pattern. The mean field solutions assume $v_{max} = 1$ and simulated results are provided at $v_{max} = 1$. Normally, $v_{max} = 5$ is considered to be more realistic [Nagel & Schreckenberg 1992] so simulated results are also provided at $v_{max} = 5$.

6.1.1 Flow-vs-left-turn proportion

Left-turning traffic (L) has the most negative effect on flow (compared to right-turning and nonturning traffic) in the mean field approximation and simulated results (Figure 6.1. The

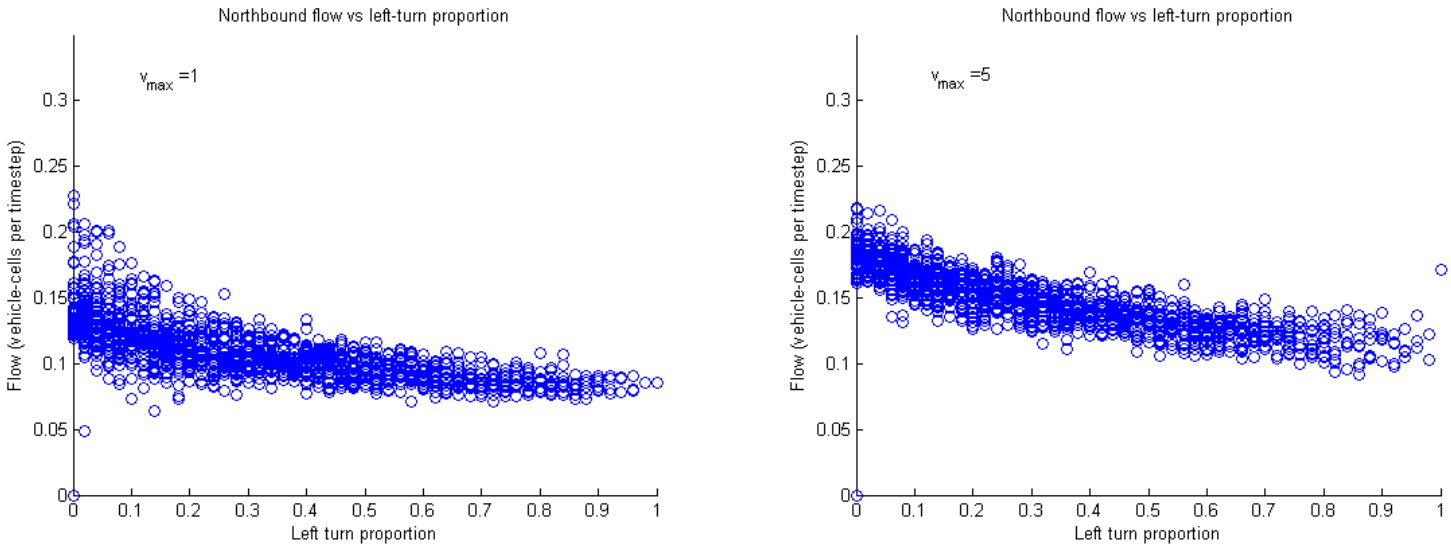

Figure 6.1: Flow-vs-left-turn proportion, simulated

mean-field approximation overestimates simulated flow at turn proportions above $L = 0.2$ (Figure 6.2) and underestimates below.

6.1.2 Flow-vs-right-turn proportion

In simulation (Figure 6.4), right-turning traffic has a strong positive effect on traffic flow. A sharp upward slope at very high right-turning proportions in simulation could indicate that right-turning traffic is inhibited less by itself than by left-turning or nonturning traffic. At $v_{max} = 1$ this is expected; the intersection barely hinders pure right-turning traffic since the intersection is never occupied by conflicting traffic. A small proportion of nonright-turning traffic is sufficient to force right-turning vehicles to wait through traffic lights. The mean-field approximation does not appear to capture this effect (Figure 6.5). No trend is apparent in measured date (Figure 6.6).

6.1.3 Flow vs nonturning proportion

In simulation and the mean-field approximation, nonturning traffic proportion T has a nearly neutral effect on traffic flow at low velocities (Figure 6.7). The effect of increasing T is

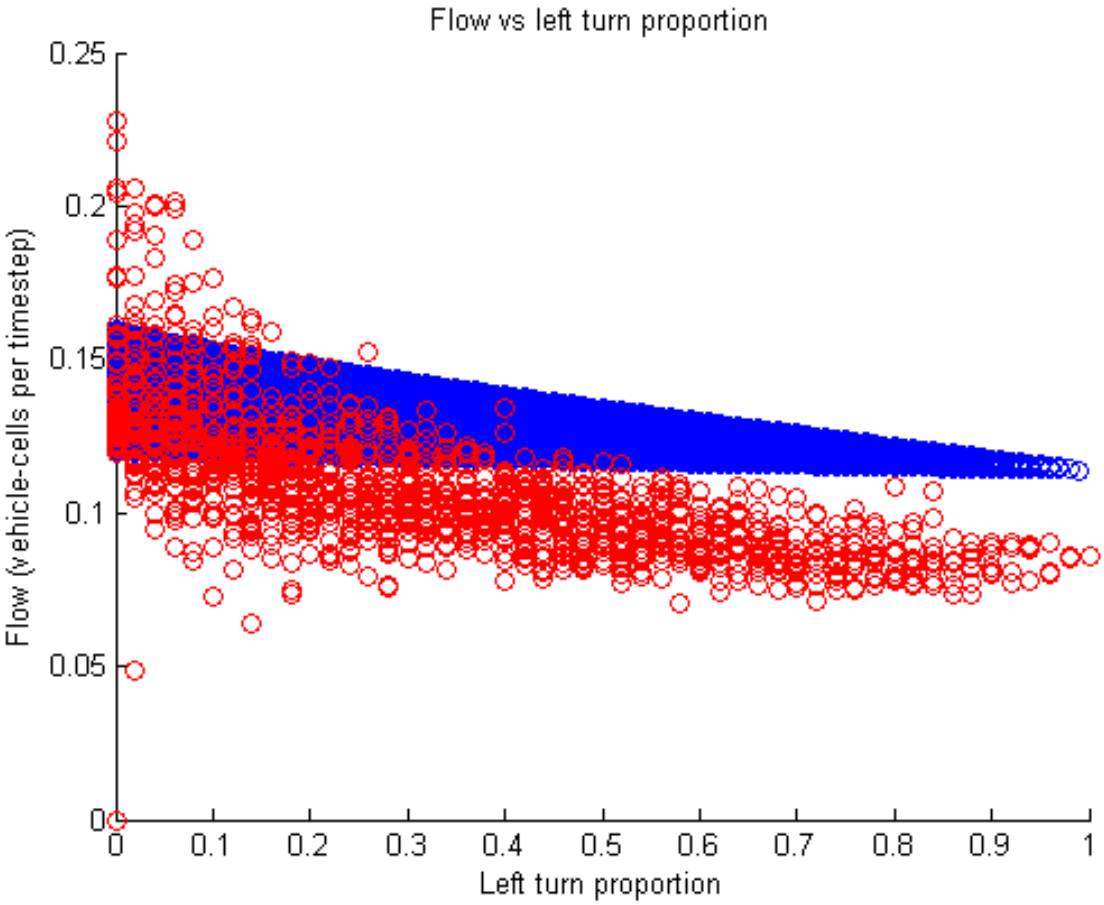

Figure 6.2: Mean-field and simulated comparison of flow vs. left turn proportion(red: simulated, blue: mean field)

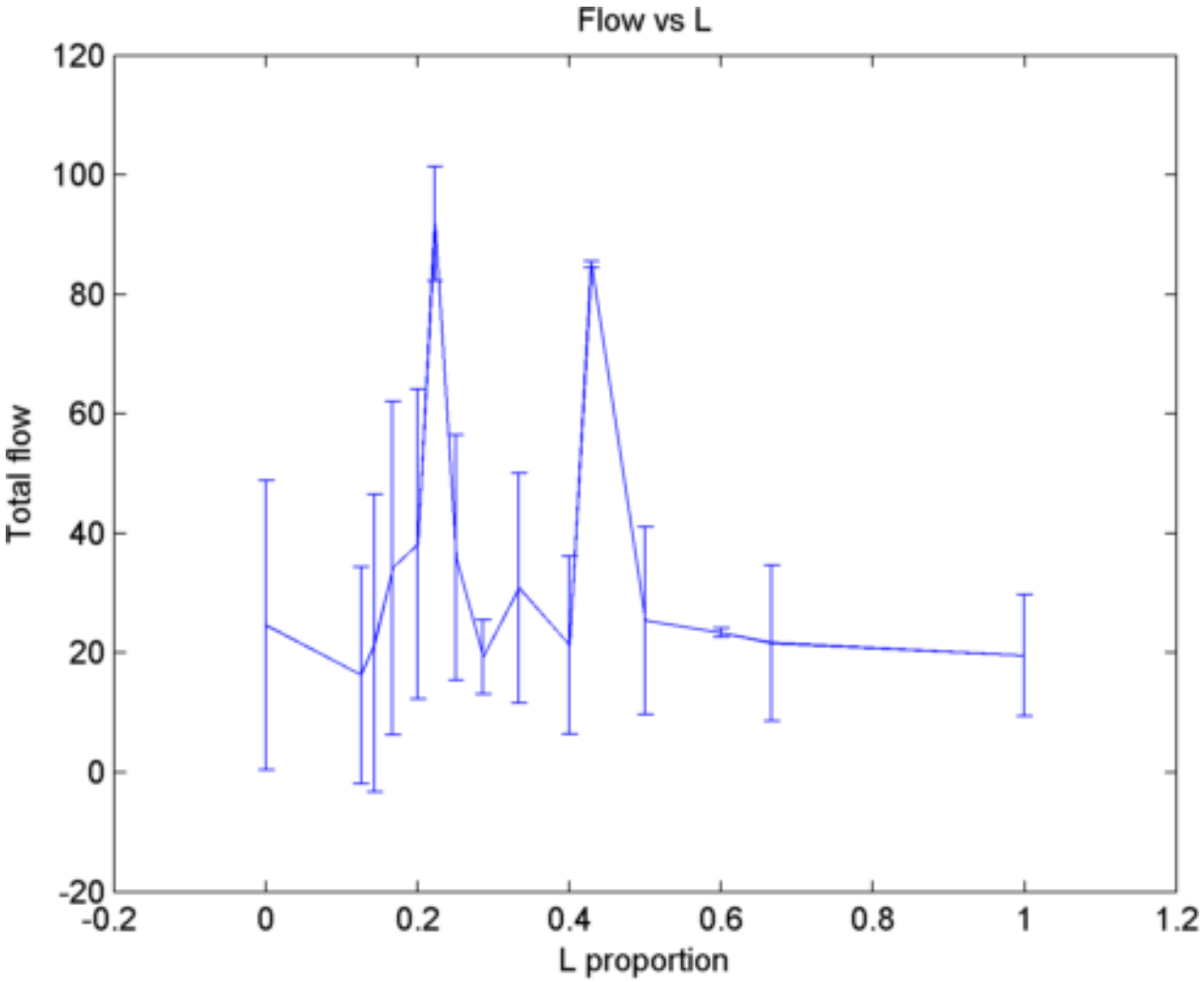

Figure 6.3: Measured flow vs left-turn proportion. Error bars show one standard deviation of measurement spread.

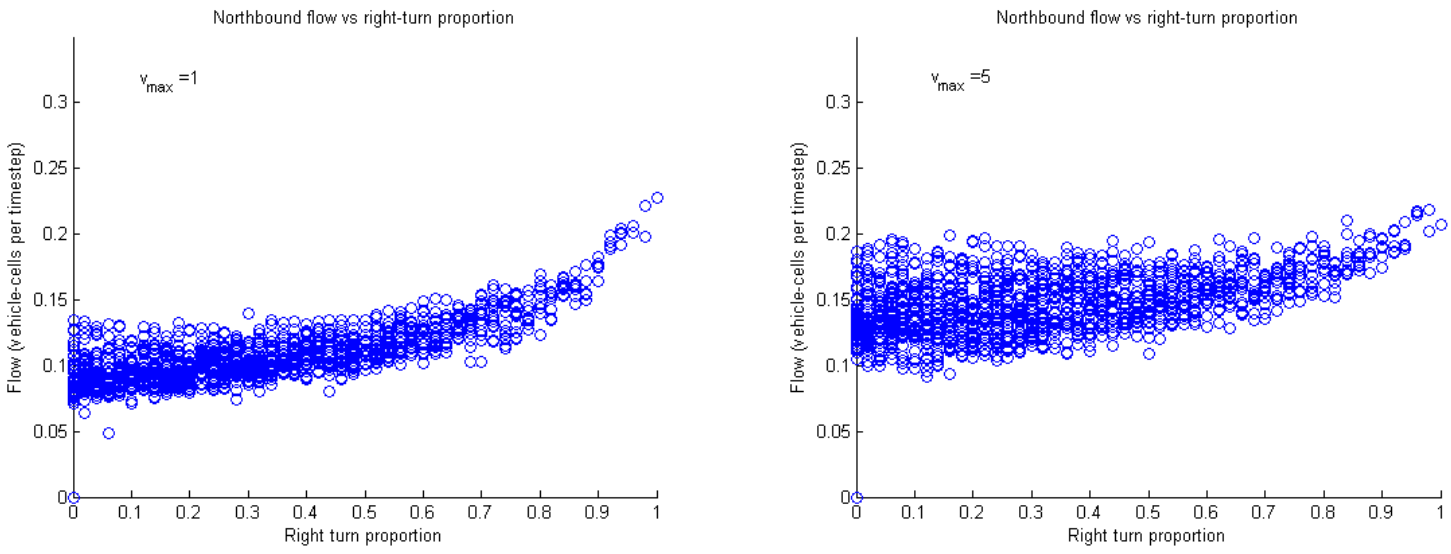

Figure 6.4: Flow vs right-turn proportion, simulated

positive at higher velocities. At $v_{max} = 5$, nonturning traffic has the advantage of not being required to stop at the intersection while turning traffic is required to stop at least once. The cost of stopping is minimal for $v_{max} = 1$ and so at low speed, right turning traffic is not at a significant disadvantage compared to nonturning traffic. The mean-field approximation appears to slightly overestimate simulated flow rates except at very low values of T (Figure 6.8). No relationship is apparent in Figure 6.9.

6.1.4 Two dimensional flow vs turn proportion

The flow rate as a function of turn proportions L and R can be visualized as a triangle in the $L - R$ plane. Flow rate is indicated by intensity; the highest flow rate in simulation is at $R = 1$ in the upper right corner (Figure 6.10). The mean-field results for $v_{max} = 1$ resemble the simulated results and the measured data displays a similar trend although sampling is sparse (6.11); more measurements would be necessary to clearly visualize the relationship. Simulation agrees fairly well with the MFA results (which generally overestimates the simulated flow rates). At low values of L and high values of R, the situation is reversed: the MFA underestimates simulated flow rates. In general, the video-based measurements are very

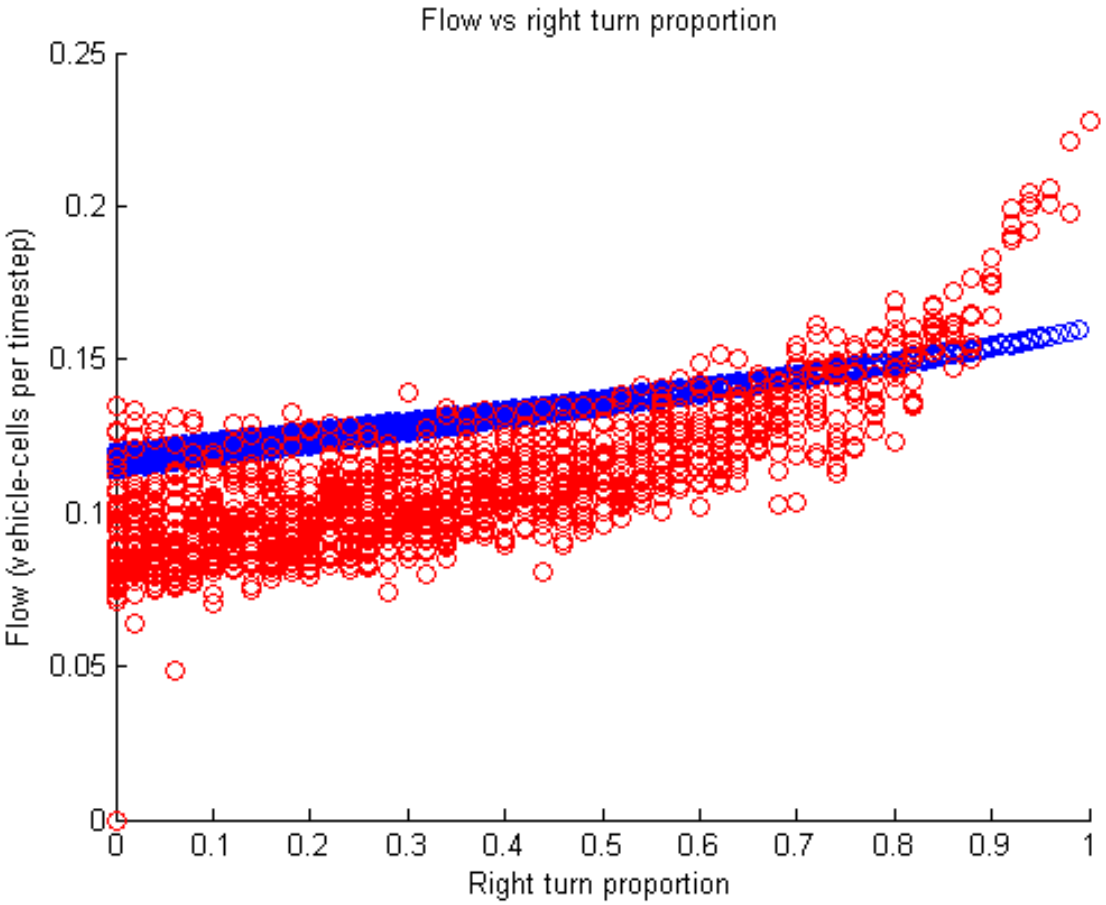

Figure 6.5: Mean-field and simulated comparison of flow vs. right turn proportion(red: simulated, blue: mean field)

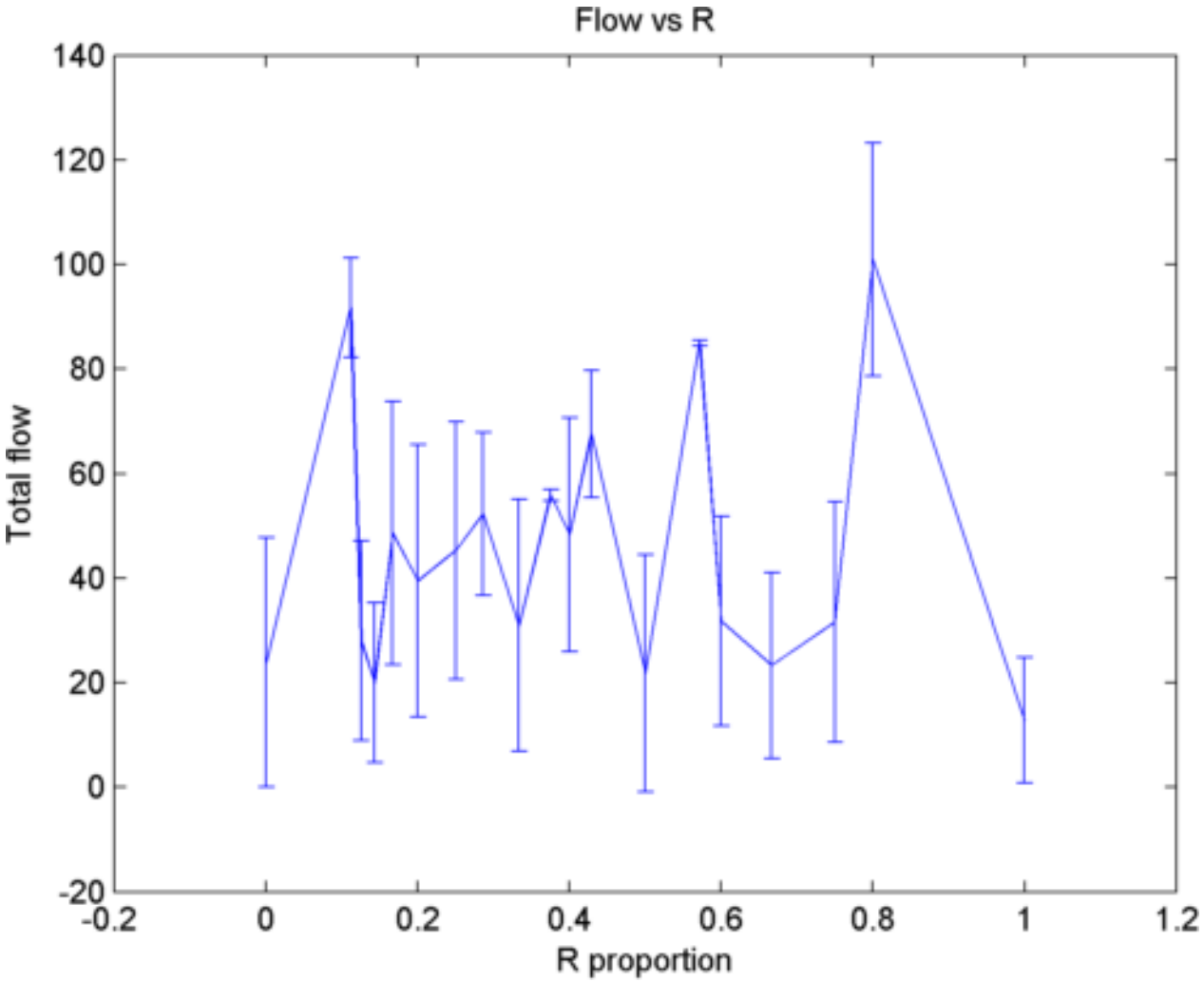

Figure 6.6: Measured flow vs right-turn proportion. Error bars show one standard deviation of measurement spread.

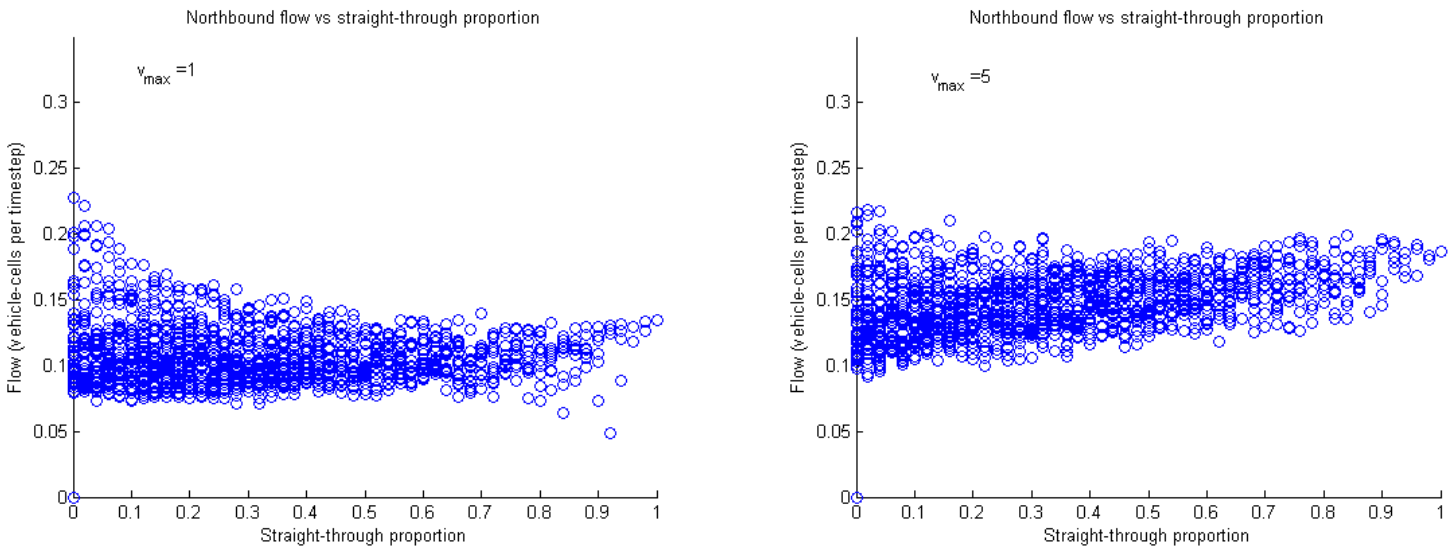

Figure 6.7: Flow vs straight-through proportion

scattered implying the presence of other factors which dominate the effect of turn proportion, at least over the time-scale considered.

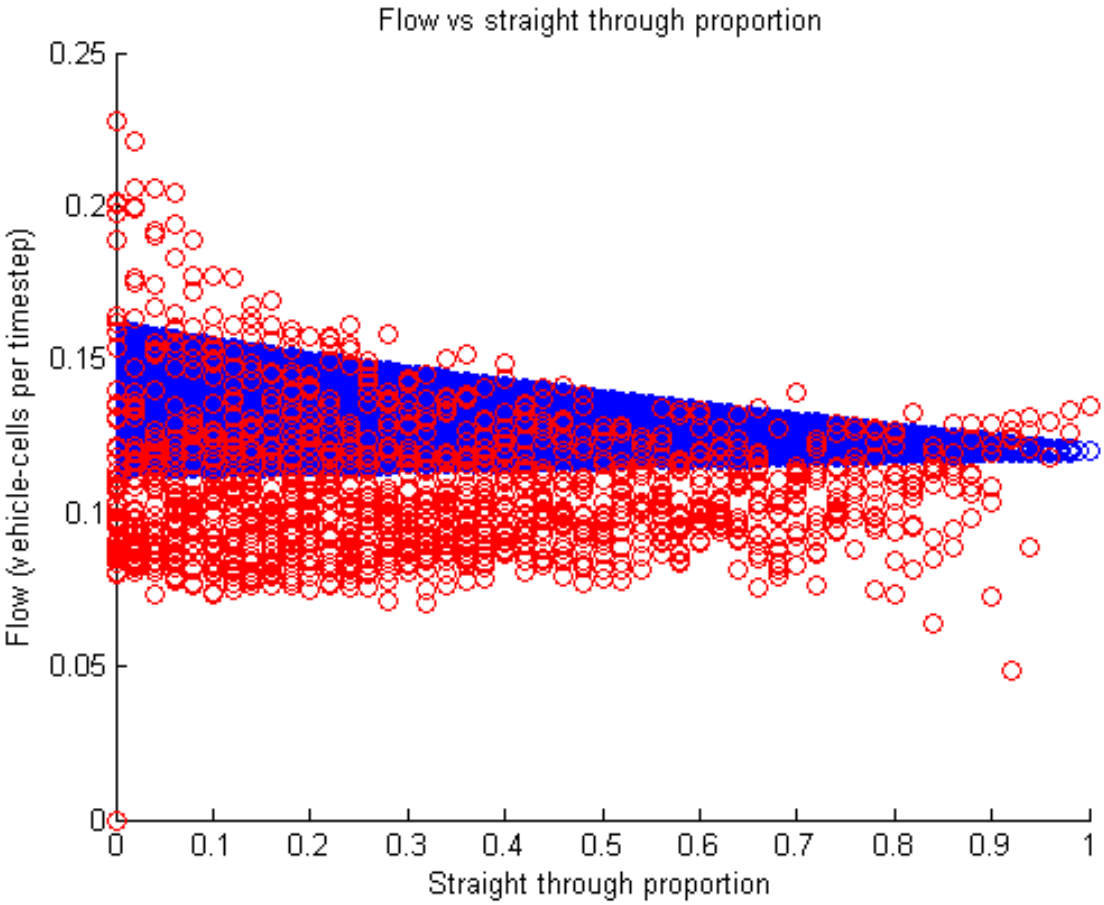

Figure 6.8: Mean-field and simulated comparison of flow vs. straight through proportion(red: simulated, blue: mean field)

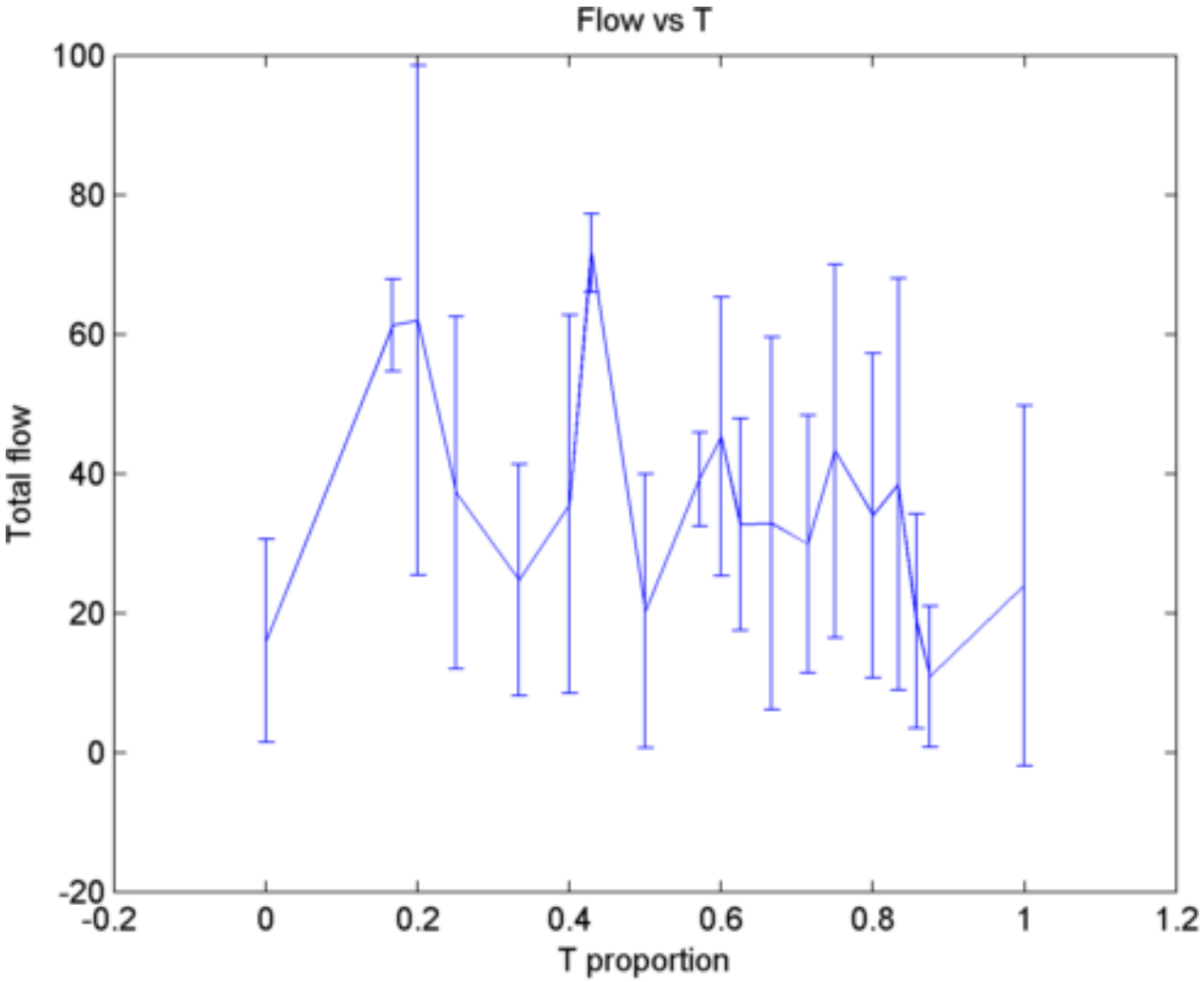

Figure 6.9: Measured flow vs straight-through proportion. Error bars show one standard deviation of measurement spread.

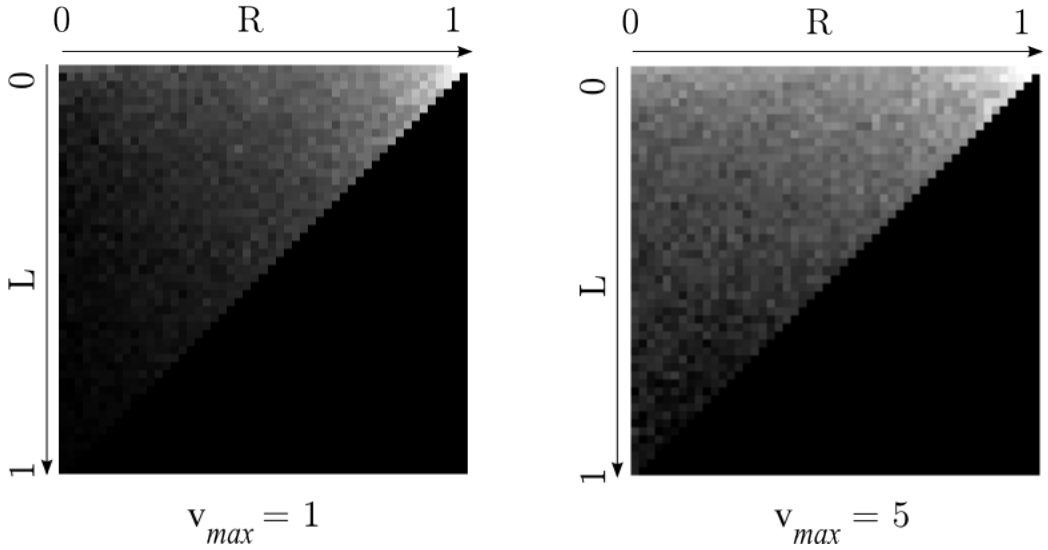

Figure 6.10: Flow vs LR plane, simulated

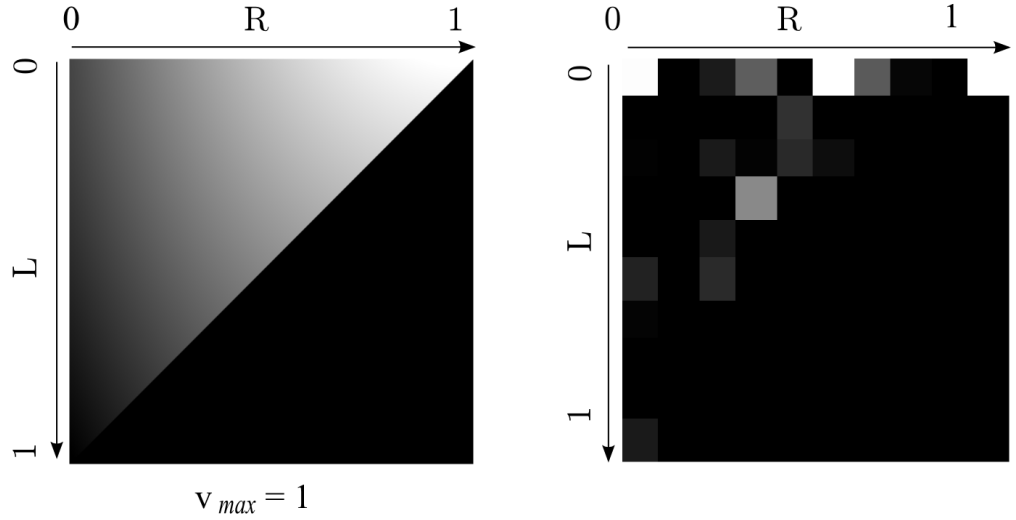

Figure 6.11: Mean field approximation (left) and empirical sampled (right) on L-R plane

Chapter 7

Concluding Remarks

7.1 Discussion

The intersection model presented here attempts to represent the effects of turning traffic more realistically than existing models. The mean-field approximation, a common tool in CA model analysis, is applied here to characterize the effects of turn proportion in this model that previous models often lack. Based on the wide scatter of the measured data, it appears that either the flow rates are not strongly influenced by the turn proportion as an average quantity over the time scale of interest or the video measurement methods are too inaccurate to discern the effect. Longer measurements might yield a clearer relationship. The mean-field approximation and simulation may still be useful as a way to roughly examine the long-term effects of alternative traffic rules.

The video-based vehicle tracking and turn detection software has potential for improvement. No large barrier exists to real-time implementation. More complex pedestrian and vehicle movement models could assist in classification and tracking. With a high viewpoint and during daylight, this system could provide higher-quality feedback than more expensive alternatives like inductive loops. However, requiring a camera to be located on a tall building

is inconvenient - a ground-level sensor would be preferable. Ground-level cameras must deal with additional problems; perspective distortion (nearer objects appear larger), overlap, smaller field of view. However, in principle the sample low-level blob detection and multiple object tracking methods could be applied. Vehicle detections from multiple ground-level cameras could be projected onto a shared image, providing the necessary field of view without requiring a difficult vantage point. Calibration of the cameras to the shared image is another additional difficult not present using the higher vantage point.

7.1.1 Sources of error

The video-based vehicle tracking error is high; a wide variety of movement and object types in the frame cause problems for fixed blob-based MHT. Frequent error types include trackers switching vehicles; multiple trackers being assigned to a single vehicle; pedestrians being mistaken for vehicles and vice versa.

One problem with directly comparing the mean-field and simulated results to the measured results is the difficulty of empirically sampling flow rates evenly at all possible turn proportions. The true distribution of flow-vs-turn-proportion samples is a product of the flow-vs-(L, R) surface and the distribution of (L, R) values that occur at the intersection. Treating the (L, R) as a process instead of a fixed value in simulation might yield results closer to the actual distribution.

Another factor affecting comparison of the measured and simulated results is the time scale. The measurements were taken from videos over a 2-hour period while simulations can represent hundreds or thousands of hours. This implies that at least in the short term, turn proportions are not a major component of intersection dynamics. The existing intersection models are therefore somewhat justified in neglecting certain interactions inside the intersec-

tion in favor of simplicity.

Relaxing the symmetry assumptions may improve results quantitatively at the cost of clarity. However, after relaxing enough simplifying assumptions, full microsimulation of an intersection system on a vehicle-by-vehicle basis might become an attractive option. Some quantities may not be useful to considered true macroscopic variables at relevant geometric or time scales.

7.2 Future directions

7.2.1 Intersection Models

The lack of a clear measured relationship between turn proportions and flow rates indicates that treating L, R, T as macroscopic variables may not be worthwhile. Detailed microsimulations make fewer assumptions. In some situations (with very high numbers of particles and long time scales of interest), the computational difficult of particle-level simulations is unrealistic. However, in the case of traffic, real-time simulation of individual vehicles is possible. In this case, models for individual vehicles' behaviour might be more important than abstractions describing the intersection as one unit.

7.2.2 Video-based vehicle tracking

The video-based tracking system has significant potential for improvement. Interacting Multiple Model (IMM) Kalman filters could help distinguish between pedestrians, various vehicle trajectories, cyclists and other moving objects that commonly occur in intersections. Segmentation of the image into road and sidewalk could improve object tracking and detection by using a geometric model of object occurance probability. Each vehicle's full trajectory information (instead of endpoints) could be used in turn classification. Now, only the initial and final vehicle locations are used. Using the entire trajectory for turn classification would

eliminate errors caused by a tracker initializing or disappearing in the wrong location (a fairly common occurance since vehicle deletion and detection tends to occur in the same narrow regions at the edge of the image). The implementation of MHT in this case does not split and join paths; this can yield significant increases in look-ahead ability for the object tracker which would result in an overall improvement of accuracy.

Bibliography

Biham, O., Middleton, A. & Levine, D. Self-organization and a dynamical transition in traffic-flow models. *Physical Review A*, 46(10):6124–6127 [1992]. ISSN 1094-1622. URL:http://link.aps.org/doi/10.1103/PhysRevA.46.R6124

Blackman, S. Multiple hypothesis tracking for multiple target tracking. *IEEE Aerospace and Electronic Systems Magazine*, 19(1):5–18 [2004]. doi:10.1109/MAES.2004.1263228. URL:http://ieeexplore.ieee.org/lpdocs/epic03/wrapper.htm?arnumber=1263228

Brockfeld, E., Gartner, N., Sohr, A. & Wagner, P. Fundamental diagram on urban roads-myth or truth? *Symposium on the Fundamental Diagram: 75 Years (Greenshields 75 Symposium)*, pages 1–5 [2008]. <m:note/>.
URL:http://www.tft.pdx.edu/greenshields/papers/C4_Wagner_abstract.pdf

Chandler, R. E., Herman, R. & Montroll, E. W. Traffic dynamics: Studies in car following. *Operations Research*, 6(2):165–184 [1958].

Chopard, B., Luthi, P. & Queloz, P. Cellular automata model of car traffic in a two-dimensional street network. *Journal of Physics A: Mathematical and General*, 29:2325 [1996].
URL:http://iopscience.iop.org/0305-4470/29/10/012

Chowdhury, D., Santen, L. & Schadschneider, A. Statistical physics of vehicular traffic and some related systems. *Physics Reports*, 329(4-6):199–329 [2000]. <m:note/>. URL:http://linkinghub.elsevier.com/retrieve/pii/S0370157399001179

Cox, I. & Hingorani, S. An efficient implementation of Reid's multiple hypothesis tracking algorithm and its evaluation for the purpose of visual tracking. *Pattern Analysis and Machine Intelligence, IEEE Transactions on*, 18(2):138–150 [1996]. URL:http://ieeexplore.ieee.org/xpls/abs$backslash$_all.jsp?arnumber=481539

Daganzo, C. Requiem for second-order fluid approximations of traffic flow. *Transportation Research Part B: Methodological*, 29(4):277–286 [1995]. ISSN 0191-2615. URL:http://linkinghub.elsevier.com/retrieve/pii/019126159500007Z

Di Febbraro, a. & Sacone, S. Hybrid modelling of transportation systems by means of petri nets. *SMC'98 Conference Proceedings. 1998 IEEE International Conference on Systems, Man, and Cybernetics (Cat. No.98CH36218)*, 1:131–135 [1998]. doi: 10.1109/ICSMC.1998.725397. URL:http://ieeexplore.ieee.org/lpdocs/epic03/wrapper.htm?arnumber=725397

Esser, J. & Schreckenberg, M. Microscopic simulation of urban traffic based on cellular automata. *International Journal of Modern Physics C-*, 8(5):1025–1036 [1997]. <m:note/>. URL:http://www.uni-due.de/imperia/md/content/ptt/paper/1997_ca_olsim.pdf

Farhi, N., Goursat, M. & Quadrat, J. Road traffic models using petri nets and minplus algebra. *Traffic and Granular Flow'07*, 27(4):281–286 [2009]. URL:http://www.springerlink.com/index/RJ36WT416751T840.pdf

Farhi, N., Goursat, M. & Quadrat, J.-P. The traffic phases of road networks. *Transportation Research Part C: Emerging Technologies*, 19(1):85–102 [2011]. doi: 10.1016/j.trc.2010.03.011. <m:note/>.
URL:http://linkinghub.elsevier.com/retrieve/pii/S0968090X10000379

Foulaadvand, M. E. & Belbaasi, S. Simulation of traffic flow at a signalised intersection. *Time*, page 7 [2008].
URL:http://arxiv.org/abs/0809.3591

Foulaadvand, M. E. & Belbasi, S. Vehicular traffic flow at an intersection with the possibility of turning. *Journal of Physics A: Mathematical and Theoretical*, 44(10):105001 [2011]. doi:10.1088/1751-8113/44/10/105001. <m:note/>.
URL:http://stacks.iop.org/1751-8121/44/i=10/a=105001?key=crossref.4a95a48e657cf293108c8948d37fd61c

Freund, J. & Pöschel, T. A statistical approach to vehicular traffic. *Physica A: Statistical Mechanics and its Applications*, 219(1):95–113 [1995]. <m:note/>.
URL:http://www.sciencedirect.com/science/article/pii/037843719500170C

Helbing, D. Derivation and empirical validation of a refined traffic flow model. *Physica A: Statistical and Theoretical Physics*, 233(1-2):253–282 [1996]. <m:note/>.
URL:http://linkinghub.elsevier.com/retrieve/pii/S0378437196002282

Herman, R., Montroll, E., Potts, R. & Rothery, R. Traffic dynamics: analysis of stability in car following. *Operations research*, 7(1):86–106 [1959].
URL:http://www.jstor.org/stable/167596

Kanai, M. Two-lane traffic-flow model with an exact steady-state solution. *Physical Review E*, 82(6):1–7 [2010]. doi:10.1103/PhysRevE.82.066107. <m:note/>.
URL:http://link.aps.org/doi/10.1103/PhysRevE.82.066107

Kerner, B. Three-phase traffic theory and highway capacity. *Physica A: Statistical and Theoretical Physics*, 333(February 2008):379–440 [2004].
URL:http://linkinghub.elsevier.com/retrieve/pii/S0378437103009221

Kerner, B. & Konhhauser, P. Cluster effect in initially homogeneous traffic flow. *Physical Review E*, 48(4):2335–2338 [1993]. <m:note/>.
URL:http://link.aps.org/doi/10.1103/PhysRevE.48.R2335

Lawniczak, A. & Di Stefano, B. N. Development of road traffic ca model of 4-way intersection to study travel time. *Complex Sciences*, pages 2040 – 2049 [2009]. <m:note/>.
URL:http://www.springerlink.com/index/l0896841676171l2.pdf

Levine, E., Ziv, G., Gray, L. & Mukamel, D. Phase transitions in traffic models. *Journal of Statistical Physics*, 117(5-6):819–830 [2004]. doi:10.1007/s10955-004-5706-6. <m:note/>.
URL:http://www.springerlink.com/openurl.asp?id=doi:10.1007/s10955-004-5706-6

Lighthill, M. & Whitham, G. On kinematic waves. II. A theory of traffic flow on long crowded roads. *Proceedings of the Royal Society of London. Series A. Mathematical and Physical Sciences*, 229(1178):317 [1955]. ISSN 1364-5021.
URL:http://rspa.royalsocietypublishing.org/content/229/1178/317.short

Maerivoet, S. & De Moor, B. Cellular automata models of road traffic. *Physics Reports*, 419(1) [2008]. <m:note/>.

Murty, K. An algorithm for ranking all the assignments in order of increasing cost. *Operations Research*, 16(3):682–687 [1968].
URL:http://www.jstor.org/stable/168595

Nagatani, T. Shock formation and traffic jam induced by a crossing in the id asymmetric exclusion model. *J. Phys. A*, 26(23):6625–6634 [1993].

Nagel, K. & Schreckenberg, M. A cellular automaton model for freeway traffic. *Journal de Physique I*, 2(12):2221–2229 [1992].
URL:http://hal.archives-ouvertes.fr/docs/00/24/66/97/PDF/ajp-jp1v2p2221.pdf

O'Loan, O., Evans, M. & Cates, M. Jamming transition in a homogeneous one-dimensional system: The bus route model. *Physical Review E* [1998]. <m:note/>.
URL:http://pre.aps.org/abstract/PRE/v58/i2/p1404_1

Prigogine, I. & Andrews, F. C. A boltzmann-like approach for traffic flow. *Operations Research*, 8(6):789–797 [1960]. doi:10.1287/opre.8.6.789. <m:note/>.
URL:http://or.journal.informs.org/cgi/doi/10.1287/opre.8.6.789

Reid, D. An algorithm for tracking multiple targets. *IEEE Transactions on Automatic Control*, 24(6):843–854 [1979]. ISSN 0018-9286. doi:10.1109/TAC.1979.1102177.
URL:http://ieeexplore.ieee.org/lpdocs/epic03/wrapper.htm?arnumber=1102177

Rickert, M. & Nagel, K. Experiences with a simplified microsimulation for the Dallas/Fort Worth area. *Arxiv preprint adap-org/9705002*, pages 1–20 [1997].
URL:http://arxiv.org/abs/adap-org/9705002

Rosenblueth, D. & Gershenson, C. A model of city traffic based on elementary cellular automata. *Complex Systems* [2011]. <m:note/>.
URL:http://scholar.google.com/scholar?hl=en&btnG=Search&q=intitle:A+Model+of+City+Traffic+Based+on+Elementary+Cellular+Automata#0

Ruskin, H. & Wang, R. Modeling traffic flow at an urban unsignalized intersection. *Computational Science—ICCS 2002*, pages 381–390 [2002].
URL:http://www.springerlink.com/index/jkdenx404w6rf6ah.pdf

Schadschneider, A., Chowdhury, D., Brockfeld, E., Klauck, K., Santen, L. & Zittartz, J. A new cellular automata model for city traffic. *Traffic and Granular Flow '99*, 1 [1999].

Schadschneider, A. & Schreckenberg, M. Garden of eden states in traffic models. *Journal of Physics A: Mathematical and General*, 31(11):L225–L231 [1998]. doi: 10.1088/0305-4470/31/11/003.
URL:http://stacks.iop.org/0305-4470/31/i=11/a=003?key=crossref.c3f8f0e8decb8a17bd93cfc99301cbea

Schreckenberg, M., Schadschneider, A., Nagel, K. & Ito, N. Discrete stochastic models for traffic flow. *Physical Review E*, 51(4):2939 [1995].
URL:http://pre.aps.org/abstract/PRE/v51/i4/p2939_1

Tonguz, O., Viriyasitavat, W. & Bai, F. Modeling urban traffic: A cellular automata approach. *IEEE Communications Magazine*, 47(5):142–150 [2009]. ISSN 0163-6804. doi:10.1109/MCOM.2009.4939290.
URL:http://ieeexplore.ieee.org/lpdocs/epic03/wrapper.htm?arnumber=4939290

Velasco, R. & Marques, W. Navier-stokes-like equations for traffic flow. *Physical Review E*, 72(4):1–9 [2005]. doi:10.1103/PhysRevE.72.046102.
URL:http://link.aps.org/doi/10.1103/PhysRevE.72.046102

Von Neumann, J. Theory of self-reproducing automata. *IEEE Transactions on Neural Networks*, 5(1):3–14 [1966]. <m:note/>.
URL:http://scholar.google.com/scholar?hl=en&btnG=Search&q=intitle:Theory+of+Self-Reproducing+Automata#0

Wolfram, S. Cellular automaton fluids 1 : Basic theory. *Journal of Statistical Physics*, 45(3/4):471–526 [1986].

Wolfram, S. Elementary cellular automata [2012]. http://atlas.wolfram.com/01/01/184/.